Geological Quarterly, 2025, 69, 6
DOI: http://dx.doi.org/10.7306/gq.1779

A record of superimposed late- and post-Variscan regional-scale tectonic events at the NE margin of the Bohemian Massif: structural evolution of the Kamionki Graben (SW Poland, Sudetes)

Aleksander KOWALSKI[1, *] and Grzegorz PACANOWSKI[2]

[1] Polish Geological Institute – National Research Institute, Lower Silesia Branch, Al. Jaworowa 19, 50–122 Wrocław, Poland; ORCID: 0000-0003-4963-3995

[2] Polish Geological Institute – National Research Institute, Rakowiecka 4, 00–975 Warszawa, Poland; ORCID: 0000-0001-9045-3262

Kowalski, A., Pacanowski, G., 2025. A record of superimposed late- and post-Variscan regional-scale tectonic events at the NE margin of the Bohemian Massif: structural evolution of the Kamionki Graben (SW Poland, Sudetes). Geological Quarterly, 69, 6; https://doi.org/10.7306/gq.1779

Associate Editor: Łukasz Gągała

Recent results of detailed geological mapping and structural analysis complemented by 2D Electrical Resistivity Tomography (ERT) and 2D Seismic P-wave Refraction Tomography (SRT-P) are used to propose a new structural model for the polyphase evolution of the Kamionki Graben (NE Bohemian Massif). This intriguing tectonic structure is composed of syn- to late-orogenic Mississippian („Culm") strata, which represent an outlier surrounded entirely by the metamorphic rocks of the Góry Sowie Massif. The Kamionki Carboniferous succession was folded (and, locally, also probably thrusted over the gneissic basement) into the WNW–ESE to W–E and, less commonly, NW–SE oriented folds during the late Mississippian (early Namurian?) Epoch. The graben development only slightly postdated the folding of the Carboniferous and we correlate it with significant regional uplift and erosion, which was related to the late-orogenic gravitational collapse of the newly formed Variscan orogen. Hence, the main boundary faults of the graben may have been genetically linked with a late Carboniferous–early Permian extensional (transtensional?) episode at the NE Bohemian Massif. The structure of the graben was later reshaped during the Late Cretaceous–early Paleogene trans-regional tectonic shortening event, which likely led to the reactivation of the main boundary faults of the graben as well as large-scale, gentle folding of the strata, visible only in map-view, especially in the northern parts of the graben. The later, Neogene (?), NE–SW-oriented extensional regime resulted in the formation of normal faults and it was responsible for the distinct compartmentalization of the graben. Our study provides the first description of the internal structure, fault pattern and kinematic evolution of the Kamionki Graben. Strong lithological contrasts between the sedimentary infill of the graben and its crystalline shoulders and floor makes the seismic and resistivity geophysical methods a valuable tool for investigation of its internal structure.

Key words: palaeostress, tectonic inversion, Sudety Mts., Variscan orogeny, Alpine inversion.

INTRODUCTION

The elevated area situated at the NE margin of the Bohemian Massif (BM), located between the Sudetic Marginal Fault in the NE and the Upper Elbe Fault Zone in the SW (Fig. 1), referred to as the Sudetic Block (e.g., Don and Żelaźniewicz, 1990; Aleksandrowski et al., 1999; Kryza et al., 2004; Mazur et al., 2006), exposes a mosaic of fault-bounded, repeatedly deformed, Variscan crystalline basement units overlain by unmetamorphosed rocks of lower Carboniferous (Mississippian) to Upper Cretaceous age. In this area, these sedimentary-volcanic successions are preserved within large-scale synclinorial structures as well as in smaller, but still kilometre-scale grabens (Don and Żelaźniewicz, 1990; Solecki, 1994; Głuszyński and Aleksandrowski, 2022). These features are usually downthrown or downfolded into the Variscan crystalline basement. Apart from the two main synclinorial structures located in the Sudetes, the Intra-Sudetic and the North-Sudetic synclinoria (Augustyniak and Grocholski, 1968; Nemec et al., 1982; Dziedzic and Teisseyre, 1990; Solecki, 1994), the upper Paleozoic sedimentary successions occur locally on top of the crystalline Variscan basement. Remnants of once much more widespread Carboniferous sedimentary successions are preserved on top of the Góry Sowie Massif (GSM), a high- to medium-grade metamorphic unit situated in the Central Sudetes (Grocholski, 1967; Żelaźniewicz, 1987; Cymerman, 1998).

* Corresponding author, e-mail: aleksander.kowalski@pgi.gov.pl

Received: September 16, 2024; accepted: March 8, 2025; first published online: April 29, 2025

The Carboniferous strata in these relics include incomplete, Viséan to Namurian (?) continental and marine deposits traditionally referred to as the "*Culm of the Sowie Mountains*" (Żakowa and Żak, 1962; Oberc, 1972; Łapot, 1986, 1988; Kowalski, 2024). These deposits are correlated across the GSM area and probably represent erosional relics of an originally broader, late-Variscan basin system (Narkiewicz, 2007, 2020). These folded deposits are characterized by highly reduced stratigraphic thickness with respect to their stratigraphic equivalents from the adjacent tectonic units, i.e. the Intra-Sudetic Synclinorium (Teisseyre, 1975; Dziedzic and Teisseyre, 1990; Mastalerz, 1995); Świebodzice Depression (Nemec et al., 1980; Porębski, 1981, 1990; Pluta and Górecka-Nowak, 2018) and Bardo Structure (Wajsprych, 1978; Haydukiewicz, 1990), and occur within isolated, narrow tectonic grabens or half-grabens (Oberc, 1972).

The main aim of this paper is to discuss the geometry and the structural development of the Kamionki Graben (KG), one of the most prominent tectonic grabens developed on top of the Góry Sowie Massif and filled with Mississippian strata (Oberc, 1972). Although the geology of the study area has mapped at 1:25 000 scale and the remnants of the GSM's sedimentary cover have been described in several regional studies (Żakowa, 1960, 1963; Żakowa and Żak, 1962; Łapot, 1986, 1988), the structural features have received little attention. It has been generally accepted that tectonic deformation of the Carboniferous strata involved regional folding followed by brittle faulting (Żakowa and Żak, 1962; Oberc, 1972; Łapot, 1986). However, their timing remains imprecise. The results of the recent geological mapping and structural analysis outlined in this paper shed a new light on the tectonic evolution of the Carboniferous sedimentary cover of the NE Bohemian Massif and its relationship to the metamorphic basement. Our investigations were supported by the results of shallow geophysical surveys, including 2D Electrical Resistivity Tomography (ERT) and 2D Seismic P-wave Refraction Tomography (SRT-P). These geophysical techniques have been widely and successfully applied in regional tectonic studies, including fault characterization and the imaging of individual fault zones (Suzuki et al., 2000; Caputo et al., 2003; Zhu et al., 2009; Fischer et al., 2012; Drahor and Berge, 2017; Mojica et al., 2017; Woźniak and Bania, 2019; Müller et al., 2020; Porras et al., 2022), also in the NE Bohemian Massif region (e.g., Štěpančíková et al., 2010, 2011). Our results are important in the context of discussions of the deformation style of Central Europe during the Late Cretaceous–early Paleogene inversion event which affected the western-central European foreland of the Alps and Carpathians and is of key significance for understanding the late(?) to post-Variscan structural component of the NE Bohemian Massif.

GEOLOGICAL SETTING

The study area is located in the NE periphery of the Bohemian Massif (SW Poland, the Sudetic Block) within the Góry Sowie Massif (GSM). The GSM is a fault-bounded unit, triangular in outline (Fig. 1) composed of migmatitic paragneissess, with subordinate orthogneiss, metabasite and felsic granulite bodies (Grocholski, 1967; Żelaźniewicz, 1987, 1990; Gunia, 1999; Jastrzębski et al., 2021; Tabaud et al., 2021). The paragneisses of the GSM originated probably from flysch-like greywackes as well as pelitic deposits of early to middle Cambrian age (Żelaźniewicz, 1987; Gunia, 1999; Tabaud et al., 2021), whilst the magmatic protolith of the orthogneiss is dated at late Cambrian to Early Ordovician (Kröner and Hegner, 1998; Kryza and Fanning, 2007). The rock protolith of the gneisses was metamorphosed under amphibolite facies conditions at ~380-370 Ma (Van Breemen et al., 1988), whereas the felsic granulite and peridotite bodies had undergone earlier (at ~400 Ma; Brueckner et al., 1996; O'Brien et al., 1997), ultra high pressure–high temperature (UHP–HT) granulite facies metamorphism. Metamorphic processes had ceased in the Late Devonian (Żelaźniewicz, 1987; Cymerman, 1998; Jastrzębski et al., 2021) and were followed by rapid exhumation of the massif at the end of the Devonian (Żelaźniewicz, 1987; Bröcker et al., 1998). The GSM is currently interpreted as an allochthonous terrane assigned to the Teplá-Barrandian/Bohemian microplate, located close to the northern peripheries of Gondwana during Cambrian–Ordovician (Catalán et al., 2021; Jastrzębski et al., 2021; Tabaud et al., 2021; Franke and Żelaźniewicz, 2023).

Remnants of the Mississippian sedimentary succession resting on top of the GSM are known only from the uplifted Sowie Mts. Block located to the southwest of the Sudetic Marginal Fault (Fig. 1). This succession, historically referred to as the "*Culm of the Sowie Mountains*" (Żakowa and Żak, 1962; Oberc, 1972; Łapot, 1986, 1988), is preserved within a number of small, mainly NW–SE trending, fault-bounded grabens and half-grabens. These tectonic units include the Walim, Glinno, Kamionki and Sokolec-Jugów grabens (Fig. 1). The Carboniferous strata preserved within these units include middle Viséan to Namurian(?) continental and marine deposits (Fig. 2; Żakowa, 1960, 1963; Żakowa and Żak, 1962; Muszer et al., 2016a, b). These deposits can be considered as stratigraphic equivalents of the adjacent tectonic units, i.e. the Intra-Sudetic Synclinorium (Teisseyre, 1975; Dziedzic and Teisseyre, 1990; Mastalerz, 1995), the Świebodzice Depression (Nemec et al., 1980; Porębski, 1981, 1990), and the Bardo Structure (Wajsprych, 1978; Haydukiewicz, 1990).

The Carboniferous of the GSM is 300 metres thick and has been subdivided lithologically into three informal lithostratigraphic members (Żakowa and Żak, 1962; Żakowa, 1963; Łapot, 1986). The succession begins with poorly sorted, "gneissic" and "gabbroic" conglomerates and sedimentary breccias (Fig. 3) that overlie the GSM metamorphic basement (Łapot, 1986). The name Walim Formation has been proposed for these deposits which are exposed locally over the GSM (Kowalski, 2024). The conglomerates are interpreted as deposits of alluvial fans developed along tectonically active, high-relief margins of a wider intramontane (?) basin (Kowalski, 2024). They pass upward (and possibly laterally) into marine sandstones and mudstones, up to 100 m thick. Based on macrofossils, these deposits were first dated as late Viséan (Żakowa, 1960; Żakowa and Żak, 1962) whereas Muszer et al. (2016a) suggest that they may represent the Namurian. The marine sandstones and mudstones were previously informally assigned to the Sokolec Beds (Żakowa, 1966) and currently are referred to as the Sokolec Formation (Kowalski, 2024). The uppermost member of the Carboniferous succession in the GSM consists of an ~80 m-thick, Namurian(?) polymictic conglomerate, well exposed in the central and northern sectors of the Kamionki Graben (Żakowa and Żak, 1962) and within the Sokolec-Jugów Graben (not described here). The conglomerate, assigned to the Kamionki Formation, is interpreted as deposited by fan deltas which entered the early Carboniferous basin from the north and north-west (Kowalski, 2024).

The tectonic setting of the Kamionki Graben is, as yet, not well understood. There are only two boreholes that drilled through the Carboniferous succession and reached its metamorphic basement at depths of 110 and 143 m, respectively. Moreover, these boreholes postdated the detailed field mapping made by Dathe (1902), Żakowa and Żak (1962) and

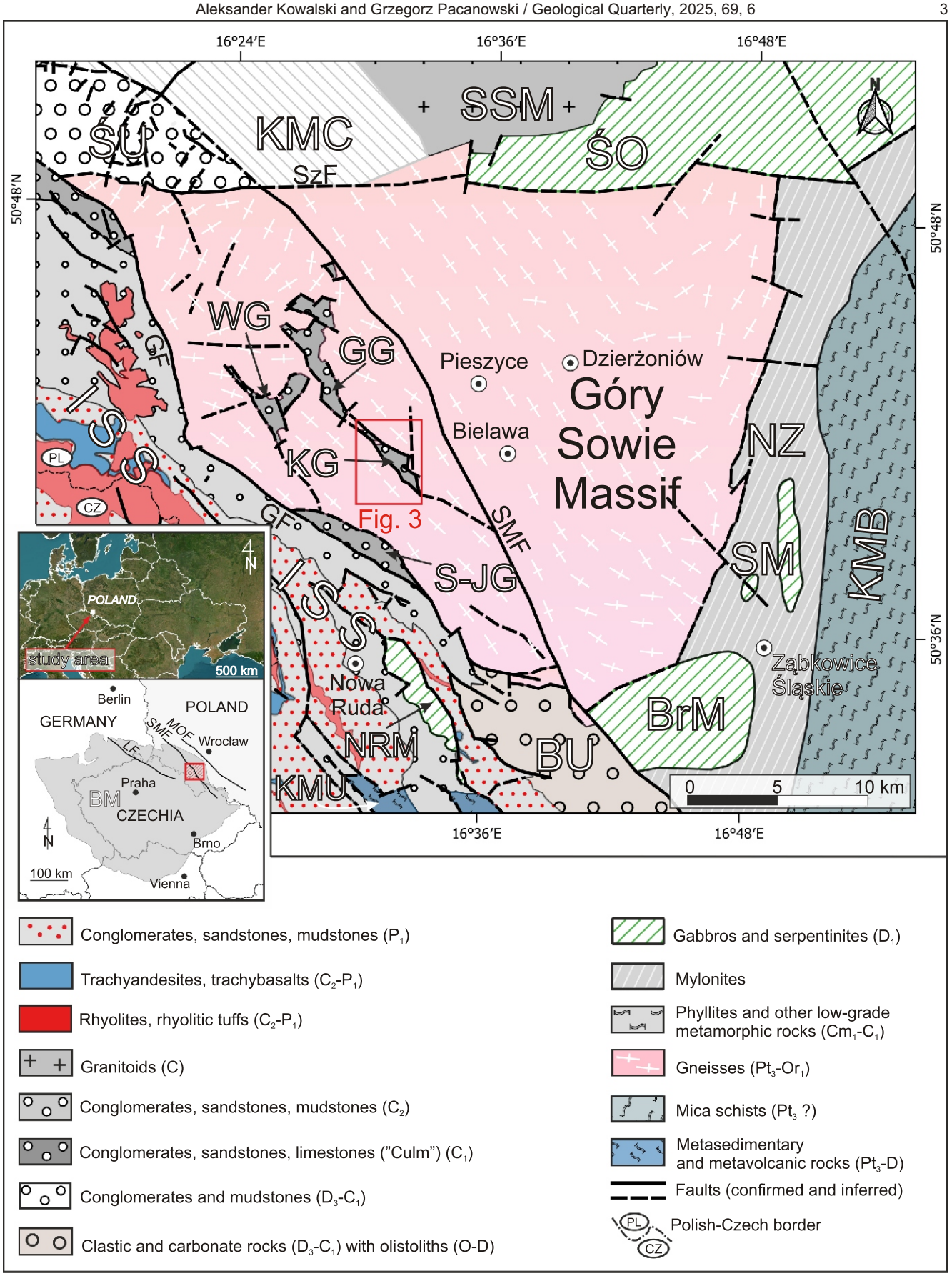

Fig. 1. Tectonic sketch map of the Góry Sowie Massif and surrounding tectonic units, together with their location in the Bohemian Massif and Central Europe (inset)

BrM – Braszowice Ophiolite Massif, BU – Bardo Unit, GG – Glinno Graben, ISS – Intra-Sudetic Synclinorium, KG – Kamionki Graben, KMB – Kamieniec Metamorphic Belt, KMC – Kaczawa Metamorphic Complex, KMU – Kłodzko Metamorphic Unit, NRM – Nowa Ruda Ophiolite Massif, NZ – Niemcza Shear Zone, S-JG – Sokolec-Jugów Graben, SM – Szklary Ophiolite Massif, SSM – Strzegom-Sobótka Granitoid Massif, ŚO – Ślęża Ophiolite Massif, ŠU – Świebodzice Unit, WG – Walim Graben. Faults: GF – Głuszyca Fault, MOF – Middle Odra Fault, LF – Lusatian Fault, SMF – Sudetic Marginal Fault, SzF – Szczawienko Fault. Geological map based on Sawicki (1995), modified and supplemented by authors

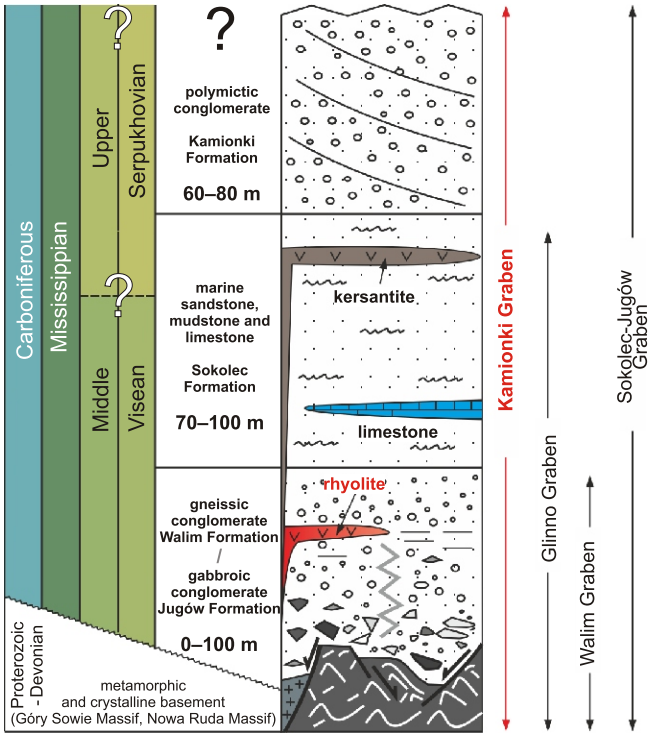

Fig. 2. Synthetic scheme showing the stratigraphy, lithology, extent and thickness of the Carboniferous succession preserved in the tectonic grabens developed on top of the Góry Sowie Massif

Gawroński (1962). The boundaries and internal structure of the graben-fill deposits were differently interpreted by these authors. For example, Dathe (1902) did not interpret fault boundaries between the Carboniferous sedimentary cover and basement in the Kamionki Trough, whilst Żakowa and Żak (1962) described the graben as a distinct, fault-controlled depression. Oberc (1972), in turn, claimed that the triangular-shaped graben was filled with Lower Carboniferous deposits and bordered by regional fault zones rooted in the crystalline basement. He labelled these faults as the "Western Kamionki-Michałkowa Fault" (western boundary fault), the "*Eastern Kamionki-Michałkowa Fault*" and the "*Pniaki-Rościszów Dislocation*" (eastern boundary faults).

MATERIAL AND METHODS

This paper is based on a new geological mapping and structural study, combined with 2D Electrical Resistivity Tomography (ERT) and 2D Seismic P-wave Refraction Tomography (SRT) geophysical surveys which have been used to reconstruct the long-term development of the Kamionki Graben.

MAPPING SURVEY AND STRUCTURAL FIELD STUDY

The field mapping survey covered an area of an area of ~10 km^2 and was facilitated by the use of LiDAR-based (*Light Detection and Ranging*) digital elevation models (DEMs) with 1 x 1 m resolution. The elevation data were acquired through airborne laser scanning (ALS), conducted in Poland in 2011–2014 as part of the IT System of the Country's Protection against Extreme Hazards (ISOK) programme. The results of the scanning were made available by the Polish Centre of Geodetic and Cartographic Documentation (CODGiK) as XYZ point data, with a density of ~4–6 point/m^2 and an average elevation error not exceeding 0.3 m (Wężyk, 2015). The DEMs proved particularly useful in detecting lithological boundaries based on the classic three-point method (e.g., Compton, 1962) using GIS software: *QGIS Software v. 3.4.15* and *Microdem Software v. 2015.8* (developed by Peter Guth), as well as in interpreting specific morphological features related to tectonic activity (i.e. lineaments related to supposed faults). Two hydrogeological borehole logs from the eastern part of the Kamionki Graben were used for the construction of interpretive geological cross-sections (SPDPSH, 2024).

Field study was focused on collecting detailed structural data in natural and artificial exposures in the area of the graben and its nearest surroundings. Selected exposures were grouped into 8 representative sites (see Fig. 3 for their location). The structural features recorded included bedding (1), joints (2) and striated fault planes (3). The fractures were grouped into sets and shown on circular frequency polygon plots (cf. Davis and Sampson, 1986). Structural analysis of faults included 32 fault planes with recognizable slip sense. The slip sense was determined based on kinematic indicators (surface markings; Petit 1987) such as striated ridges, hackles, grooves, low- and high-angle Riedel shears, en echelon cracks and others. Fault plane orientations are shown on and stereograms made on the lower hemisphere of equal-area Schmidt-Lambert nets. The kinematic fault slip data were used to determine the successive patterns of brittle strain. Reconstructions of principal axes of the finite strain ellipsoid based on the fault population were performed using *FaultKin8* software. The strain patterns were reconstructed using the graphic analysis of fault slip data included in the kinematic method of "P" (shortening), "T" (extension) and "B" (neutral) incremental strain axes (PBT method – moment tensor analysis; cf. Angelier, 1984; Marrett and Allmendinger, 1990; Pascal, 2021). The relative ages of the deformation events were determined from the cross-cutting relationships between folds and brittle structures (fractures and faults).

GEOPHYSICAL SURVEY

Two shallow-penetration geophysical surveying methods, 2D Electrical Resistivity Tomography (ERT) and 2D Seismic P-wave Refraction Tomography (SRT-P), have been used to visualise subsurface structure and to identify fault boundaries of the Kamionki Graben. Two integrated ERT and SRT-P profiles, each of them 1,160 m in length, were measured across the KG (Lasocki et al., 2021). The original ERT and SRT-P cross-sections, obtained during the study, were shortened to 900 m for better presentation of the data acquired (see Fig. 3). This allowed us to determine the position, lateral extent and main boundaries of particular structural units within the KG as well as to characterise the fault zones inferred during the detailed field mapping.

Before the geophysical survey, precise geodetic positioning was made by marking the measurement points and assigning PL-1992 coordinates to each point. The points were marked out with an accuracy of 0.3 m by means of differential phase GNSS satellite methods. The quality of the GNSS readings allowed us to apply the satellite geodesy method to all the measurement points. In order to determine the elevation coordinates of all the documentation points, the satellite levelling method was used with implementation of the RTN kinematic method. The coordinates were registered in the *PL-EVRF2007-NH* height reference frame.

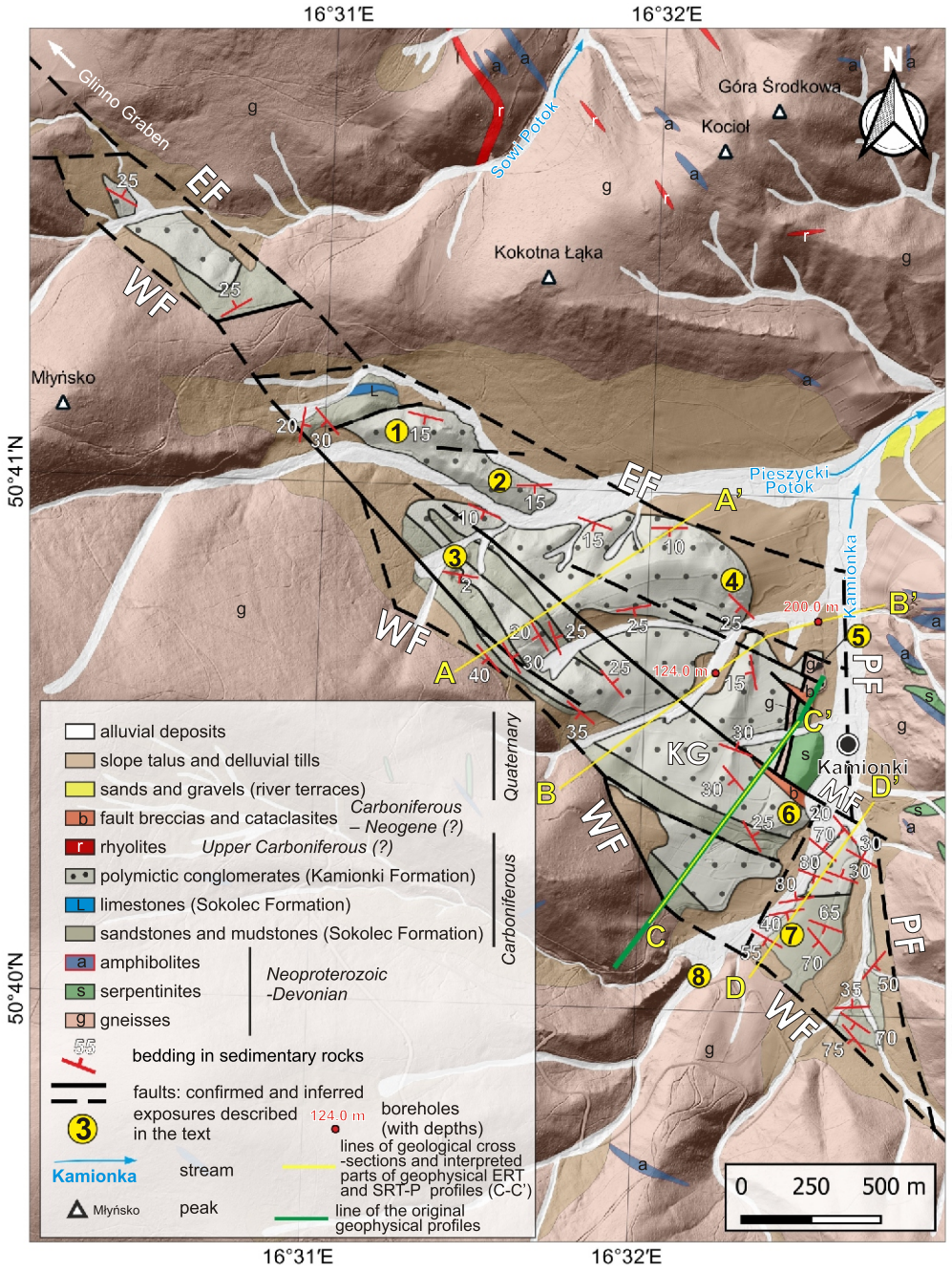

Fig. 3. Geological map of the Kamionki Graben (for location see Fig. 1)

Locations of geological cross-sections shown in Figure 4 (AA', BB', CC' and DD') and of the ERT- and SRT-P geophysical profiles from Figures 5 and 6 (CC') are indicated. Note the location of the main exposures referred to in the text and of two boreholes. Basement geology simplified from Gawroński (1961), geology of sedimentary rocks based on our own geological mapping. Abbreviations: KG – Kamionki Graben, EF – Eastern Kamionki Fault, PF – Pniaki Fault, WF – Western Kamionki Fault

2D ELECTRICAL RESISTIVITY TOMOGRAPHY

The main assumptions of the ERT method have been widely described in the literature (e.g., Keller and Frischknecht, 1966; Ward, 1987; Loke and Barker, 1996; Dahlin and Zhou, 2004; Loke et al., 2007; Loke, 2012). This geophysical technique is based on measuring artificially induced electric field parameters in a specific rock mass, as well as detecting natural currents and electrical fields caused by natural processes occurring in the Earth's crust. The basic parameter is the resistivity of the rock/soil. The unit of specific (actual) resistance is ohm-metres [m]. This parameter varies from 1 m in salt-water saturated strata to tens of thousands of m in igneous and crystalline rocks such as granites and gneisses (Ward, 1987). In comparison to other geophysical methods, the ERT method is sensitive to physical and chemical features such as temperature, density, porosity and water content, as well as the chemical and mineral composition (i.e. the presence of clay minerals) of the rock.

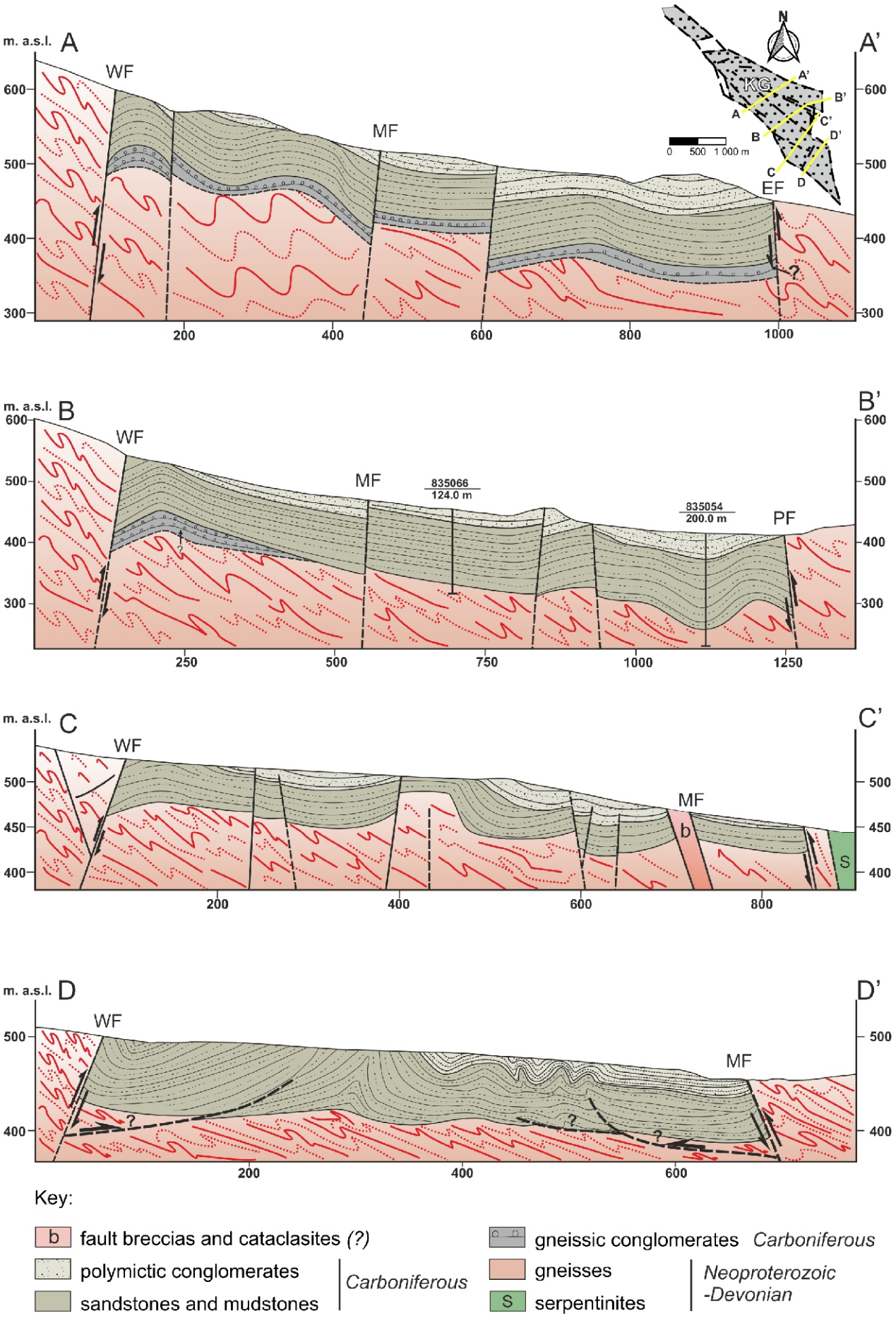

Fig. 4. Geological cross-sections across the Kamionki Graben based on mapping field traverses, borehole data and geophysical profiles shown in Figures 5 and 6 (C-C')

See inset map in the upper right corner and Figure 2 for location of each of the cross-sections
Explanations of abbreviations (faults) as in Figure 3

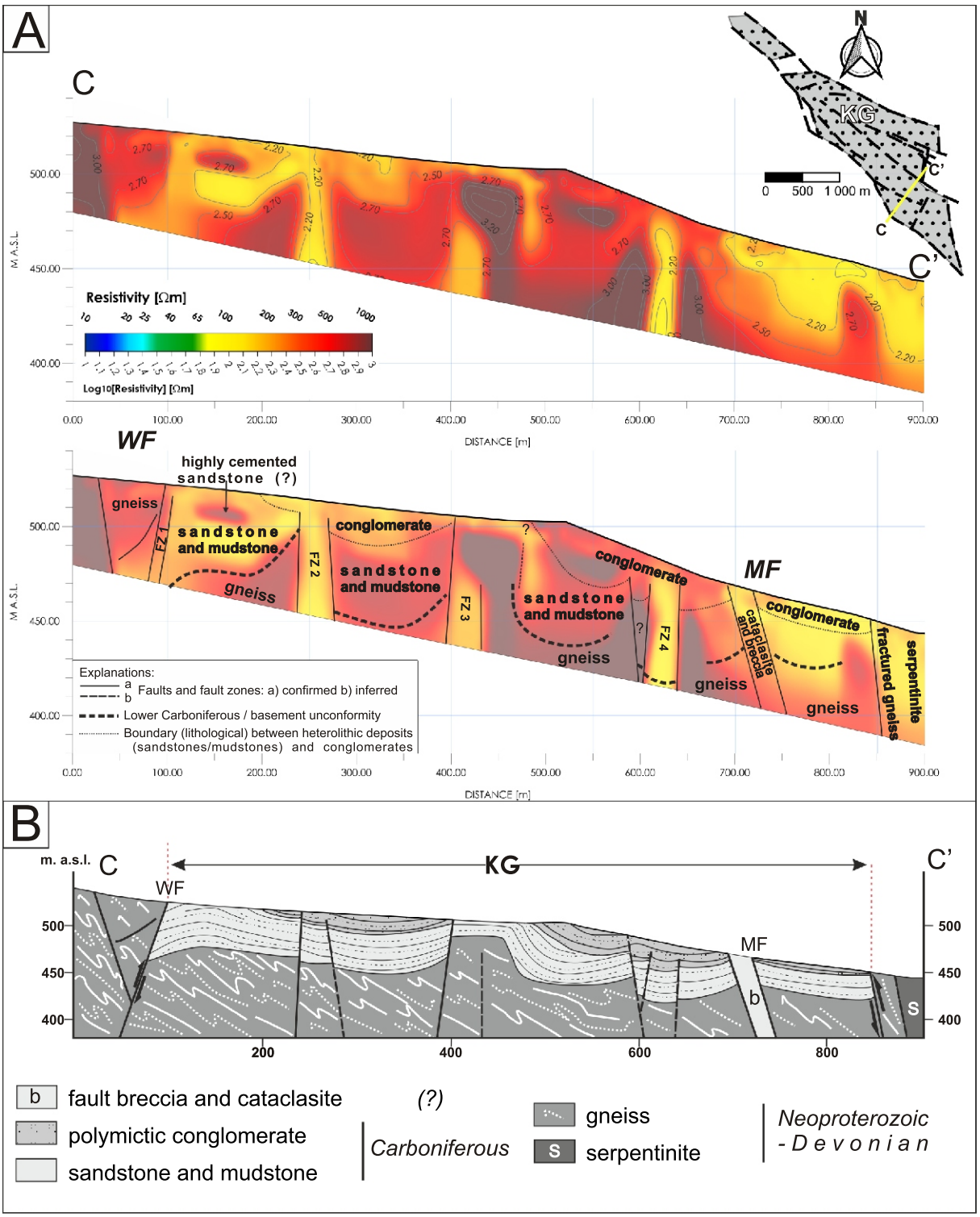

Fig. 5. 2D Electrical Resistivity Tomography (ERT) cross-section, showing interpreted resistivity values, and its geological interpretation

A – raw and geologically interpreted ERT cross-section; **B** – interpreted geological cross-section
See inset map in the upper right corner and Figure 2 for location of the CC' cross-section

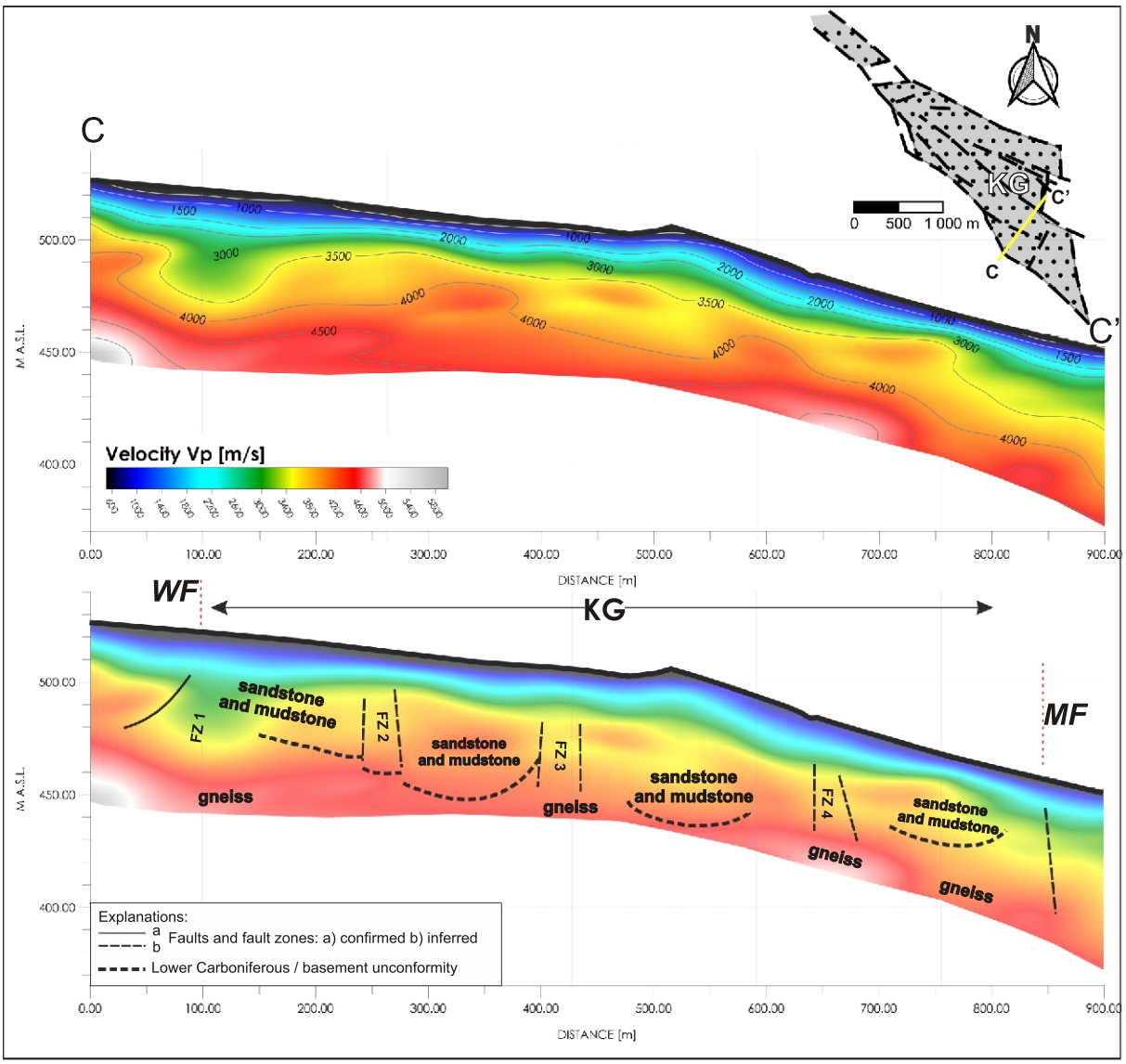

Fig. 6. 2D seismic P-wave Refraction Tomography (SRT-P) cross-section with interpretation

See inset map in the upper right corner and Figure 2 for location of the CC' cross-section

The ERT method involves placing an appropriate number of measurement electrodes along a measurement profile at regular intervals. The electrodes are connected to a multi-core cable linked to a central unit that consists of a computer-controlled electrode selector and a geoelectrical meter that enables digital recording of the measurements. The electrode selector allows for the selection of any combination of four electrodes from the entire set connected to the multi-core cable to measure apparent resistivity. After each measurement, the next set of electrodes is selected according to a pre-programmed sequence in the control computer. This allows the use of any measurement array, including the most popular configurations, such as gradient, Wenner, Wenner-Schlumberger, dipole-dipole, etc. The ERT is a common geophysical technique which has been widely used for shallow-depth detection and characterization of faults across the globe (e.g., Suzuki et al., 2000; Zhu et al., 2009; Štěpančíková et al., 2011; Drahor and Berge, 2017; Mojica et al., 2017; Porras et al., 2022).

In this study, the ERT measurements were carried out with the use of a 12-channel Terrameter LS apparatus manufactured by the Swedish company ABEM (now Guideline Geo) (ABEM, 2012). The measurements were based on a gradient array (manufacturer's measurement protocol termed the 4x21_gradient; ABEM, 2012). The active measurement setup consisted of 4 cables (each cable allowing the connection of 20 electrodes), providing a total of 80 active electrodes, with a measurement line 400 m long. The electrode spacing during the profiling was established at 5 m. The active profile consisted of 4 sections (100 m long each, which resulted in a 400 m total length of the active measuring system). Field measurements were conducted using the roll-along method, which involves moving successive cables to the front of the profile. The limitations of this method have been recently widely discussed by Pacanowski et al. (2022). Shifting the cable from the starting position to the last allows for a longer, continuous measurement profile. Such electrode spacing allowed insights into the rock

massif to a depth of ~70 m. The results of the resistivity measurements were subject to procedures of geophysical inversion with the use of Res2Dinv software (Loke, 2000), version x64 4.02.35. The inversion was performed according to the L1-norm procedure (robust, blocky).

2D SEISMIC P-WAVE REFRACTION TOMOGRAPHY (SRT-P)

The Seismic Refraction Tomography (SRT) method uses surface-generated elastic waves produced by controlled sources (the control includes both the location of the components of the measurement system – geophones and induction points – and the time of induction and of the signal recorded by the receivers; e.g., Reynolds, 2011). Due to the multiple registration of seismic waves induced at successive induction points, the measurement zone is covered with numerous seismic rays. For each induction point, the seismic wave velocity reaching each geophone is analysed. The integration of the results from all induction points includes computational, iterative fitting of the velocity model with the smallest total error (Watanabe et al., 1999). A high density of shot points, together with the use of appropriate calculation algorithms, allows determination of seismic wave velocity in the vertical section under the measurement line (Sheehan et al., 2005). This technique provides a vertical seismic wave velocity cross-section along the survey line, which allows detection of velocity anomalies, that eventually may indicate zones of weathering or possible fault zones in the rock massif (e.g., Imposa et al., 2015; Drahor and Berge, 2017; el Hameedy et al., 2023). The final result is a continuous cross-section of P- or S-wave velocity within the investigated rock massif.

The 2D Seismic P-wave Refraction Tomography (SRT-P) measurements in this study were carried out using 48-channel Terraloc Pro seismic equipment manufactured by the Swedish company ABEM (now Guideline Geo; ABEM, 2011). Geophones with a vertical component, with a natural frequency of 40 Hz, and 5 m inter-geophone spacing were used in this study (methodology in Ostrowski et al., 2023). A 10 kg sledgehammer acted as an energy source during data acquisition. Field data were processed using *Rayfract*™ software, and first arrival times were manually determined. For recordings affected by significant noise, a frequency filtering procedure was applied, enabling clear identification of the first arrivals.

RESULTS

GEOLOGICAL MAPPING

In map view, the Kamionki Graben (KG) constitutes a narrow, triangular, fault-bounded tectonic structure, ~4 km long and up to 500 m wide, which trends SE to NW to the west of the Kamionka stream valley (Fig. 3). The graben structure coincides with a morphological depression in the Góry Sowie Mountains.

The graben is formed on crystalline basement of Góry Sowie (partly migmatic paragneisses with minor serpentinite and amphibolite bodies: Gawroński, 1961; Grocholski, 1967; Fig. 3). The boundary fault zones of the graben, referred to here as the Western and Eastern Kamionki and Pniaki faults (the WF, EF and PF respectively; Fig. 3), separate the sedimentary infill of the graben from its crystalline-rock shoulders. All these fault zones are manifested by distinct rectilinear escarpments, spring lines and peat bogs. The fault zones extend laterally into the metamorphic basement of the GSM (Figs. 1 and 3). The vertical and possibly horizontal displacement components related to particular faults cannot be unambiguously determined from the mapping data. The position of the basal Carboniferous unconformity, intersected by hydrogeological boreholes at 110 and 143 m below the surface (Fig. 4), does not allow for an unequivocal determination of the vertical displacement component of the graben's floor on the boundary faults.

The geological map and cross-sections of the Kamionki Graben (Figs. 3 and 4) show the NW–SE trending faults which divide the graben's fill into several blocks. The north-westernmost part of the KG represents a single narrow NW–SE trending block (the Młyńsko Graben of Oberc, 1972) filled with Carboniferous sandstones and conglomerates and separated from the main graben body by a basement horst occuring between the WSW–ENE striking boundary faults of the graben. The northern part of the graben is characterised by the occurrence of Namurian(?) polymict conglomerates exposed along the Eastern Kamionki Fault and dipping at 15–25° towards the S and SW (Figs. 3 and 4). The structure of this part of the KG is well constrained due to exposure of the conglomerates as small-scale tors. Towards the east, the strike of the bedding within the conglomerates changes from E–W to nearly N–S. In this portion of the graben, the Pniaki Fault is oriented approximately N–S and is buried under the Kamionka stream-valley alluvial deposits (Fig. 3). The western part of the graben exposes NW-SE trending mappable folds with sandstones exposing anticline hinges (Figs. 3 and 4).

In general, the limbs of these nearly symmetrical folds dip moderately at ~25–40° towards the NE and SW with their axes plunging gently to the NW and SE (Fig. 4). The map-scale folds, oriented parallel to the structural trend of the graben, are cut by faults trending parallel or sub-parallel to the fold axes. The lowermost fill member of the KG, the gneissic conglomerate of the Walim Formation (Fig. 2), is nowhere exposed at the surface in the KG and has not been intersected by the hydrogeological boreholes made in the central part of the graben. However, the gneissic conglomerates most probably occur at the bottom of the downfaulted, northernmost part of the graben (Fig. 4, A–A' and B–B' cross sections). However, these conglomerates are well exposed within the Glinno Graben, located ~2 km towards the NW of the KG (Fig. 1; Żakowa, 1960; Oberc, 1972; Kowalski, 2024). The middle segment of the KG is dismembered by the NW-SE trending Middle Kamionki Fault (MF). This fault shows up to 50 m of throw, gradually decreasing towards the NW, and it divides the overall graben structure into two smaller domains, a southern one of almost rhomboidal shape and a northern triangular one. Geological mapping revealed the existence of distinct cataclasite zones up to 50 m wide, aligned along the southern and northern sectors of the fault zone (Figs. 3 and 4), between sedimentary rocks and their metamorphic basement. These zones consist of fault gouges and breccias of angular fragments of gneiss. To the NE of the Middle Kamionki Fault, the graben is cut by two, relatively minor, NW–SE trending discontinuities (Fig. 3). Towards the SE the KG narrows to ~50 m in width and exposes Viséan sandstones, which are folded and probably thrusted over the crystalline basement (Fig. 4, cross-section DD'). At the southernmost end of the graben, the Western Kamionki and the Pniaki faults converge to form a single, NNW-SSE striking fault.

GEOPHYSICAL SURVEY

The results of our geophysical survey are shown on two types of section: (1) a geoelectrical section, showing the calculated and geologically interpreted apparent electrical resistivity field (ERT; Fig. 5) and (2) a refraction seismic section, showing the calculated P-wave velocity field and its geological interpre-

tation (SRT-P; Fig. 6). After compilation of these geophysical sections, the cross-section so generated allowed us to constrain the subsurface geological interpretation of the graben geometry and fault arrangement, as well as to interpret the character of relationships between the graben infill and its crystalline basement (Fig. 5A, B). The geophysical profile executed was oriented roughly perpendicular to the map-view elongation of the KG and its fault boundaries (Fig. 3).

The part of the ERT section analysed, 900 m long, shows a high variability and complex pattern of apparent electrical resistivities ranging from several hundred to several thousand m (Fig. 5A). The cross-section shows distinct changes, both vertical and lateral, in the resistivity image obtained. These changes are related to different types of lithology interpreted here as the crystalline bedrock (mostly gneissic) and the graben infill. The resistivity image shows a concave-up pattern of resistivity contour lines, whose arrangement we interpret as showing mappable, large-scale NW–SE-trending fold structures within the the KG sedimentary infill (Fig. 5A). The highest resistivity values (300 to 3000 m; most commonly 500–1000 m), recorded from the SW end of the profile for about 100 metres laterally, correspond to the gneissic lithology of the south-western shoulder of the KG and of its basement, and, probably, also of strongly cemented and brecciated sandstones with low water content (Fig. 5A, B). Relatively low resistivity values were recorded in the Carboniferous sandstones and mudstones exposed at the current topographic surface. However, significant variability in resistivity values was also observed within this lithological unit. The intervals between the distance ranges from 100 to 200 m and from 250 to 600 m from the beginning of the section, while the resistivity values within sandstones range from 150 to 500 m and from ~300 to 800 m, respectively. The overlying conglomerates are characterized by low to medium resistivity values of from 300 to 3000 m. Near the end of the profile, between 850 and 900 m from its starting point, the section reveals significantly lower electrical resistivity values (around 200 m). These values correspond to strongly fractured serpentinites, gneisses, and Quaternary deposits that occur in the subsurface zone near the Kamionka River valley.

The structural interpretation was developed based on horizontal variations in the resistivity image and their correlation with the results of our geological mapping (Fig. 5B). Four narrow zones of significantly low electrical resistivity values, characterized by nearly vertical, sharp indentations, were identified. We interpret these features as fault zones (FZ-1 at a distance of 100 m from the starting point of the profile, FZ-2 at 250 m, FZ-3 at 420 m, and FZ-4 at 630 m; all of them marked by solid lines in Fig. 5A, B). The low resistivity values are regarded as corresponding to conductive, water-saturated fault zones. In addition, two narrow zones with lower resistivity values, located at distances of 710 m and 850 m on the cross-section, are interpreted as corresponding to fault breccia and cataclasite zones within the Carboniferous sedimentary rocks, as well as within the gneissic and serpentinitic bedrock identified at the surface.

The SRT-P seismic profile (Fig. 6) does not show significant changes in P-wave velocity, either near the lithological boundaries previously interpreted from mapping or at the fault zones inferred along the geoelectrical cross-section.The P wave velocity generally increases gradually with depth, without intervals of higher gradients. The cross-section shows high to very high P-wave velocity values (Vp), ranging from 3000 m/s at shallow depths to 4500–5000 m/s in the deeper parts of the profile. These values correspond to the gneiss of the basement and the southwestern shoulder of the KG. Only the near-surface Vp values (up to 10–15 m in depth) are lower than 3000 m/s, which appear to represent a weathered zone. Our seismic survey revealed a relatively homogeneous distribution of Vp values near the topographic surface, while greater variability was observed in the deeper parts of the profile. Between 50 and 200 m from the starting point of the section, much lower P-wave velocity values were recorded, likely associated with a reverse fault (?) and related brecciation. The small differences in Vp distribution correlate with the FZ1–FZ4 fault zones identified on the ERT cross-section.

STRUCTURAL ANALYSIS

MESOSCALE FOLDS

The outcrop-scale folds are relatively common deformational structures in the exposures of the Carboniferous sandstones and mudstones in the southern part of the KG. In its southernmost part (locality 7), in exposures situated along the Kamionka stream valley, a group of mesoscopic folds displays very gentle, open geometry (interlimb angles of 70–110°). Farther north, asymmetrical, N-vergent fault-propagation folds have developed, likely in the hanging wall of a thrust fault (Fig. 7A). Horizontal upright folds, tight with angular and sharp hinges, commonly with chevron-like profiles (Fig. 7B) are also present. These folds have nearly vertical axial planes, horizontal hinge lines, and involve heterolithic packages of thinly interbedded sandstone-mudstone layers. Their wavelengths range from 1 to 3 m. Additionally, asymmetrical to moderately inclined N-vergent folds, with limbs dipping nearly 80° to the S and N, are also present (Fig. 7C).

The fold axes in the Kamionki Graben predominantly trend E–W to ENE–WSW, indicating a N–S to NNE–SSW direction of tectonic shortening (Fig. 7D). The hinge zones of the anticlines occasionally display nearly vertical, planar axial cleavage. In the northern limbs of the asymmetrical folds, reverse mesofaults dipping at up to ~60° toward the NE have developed (Fig. 7D). Some minor faults were also observed. No mesoscopic folds have been identified in the sandstones exposed in the north-western part of the graben (loc. 3). In this area, a series of NW–SE-trending map-scale folds is present (cf. Figs. 3 and 4).

JOINTS AND FAULTS

The Carboniferous sedimentary rocks of the KG are affected by two (conglomerates) or three (sandstones and mudstones), conjugate sets of joints designated in this paper as J_1 to J_3 (Fig. 8A). The orthogonal or nearly orthogonal system of bed-confined joints with regular spacing, striking NW–SE (J_1) and NE-SW (J_2) is characteristic of the conglomerates exposed in the northern and central parts of the graben (loc.1 and 2). The surfaces of these joints are morphologically similar; they are usually planar, smooth and reveal apertures reaching a few millimetres (Fig. 8B). Clockwise rotation of these joints was observed in the conglomerates near the Middle Kamionki Fault (Fig. 8A, loc. 4). The combined effect of bedding and joint rotation is interpreted as the result of tectonic rotation of a fault-bounded block near the Middle Kamionki Fault, accompanied by gentle buckling. The sandstones exposed in the western part of the graben (loc. 3) are intersected by three sets of joints (Fig. 8A, C). Apart from the previously described joints of sets J_1 and J_2, there occur pervasive, well-defined joints assigned here to set J_3, striking subparallel (nearly NNW–SSE or N–S) to the graben boundaries (Fig. 8A, C). In the westernmost part of the KG, fractures show evidence of shearing in a dextral strike-slip regime (Fig. 8D). Tilted and rotated, NW–SE and

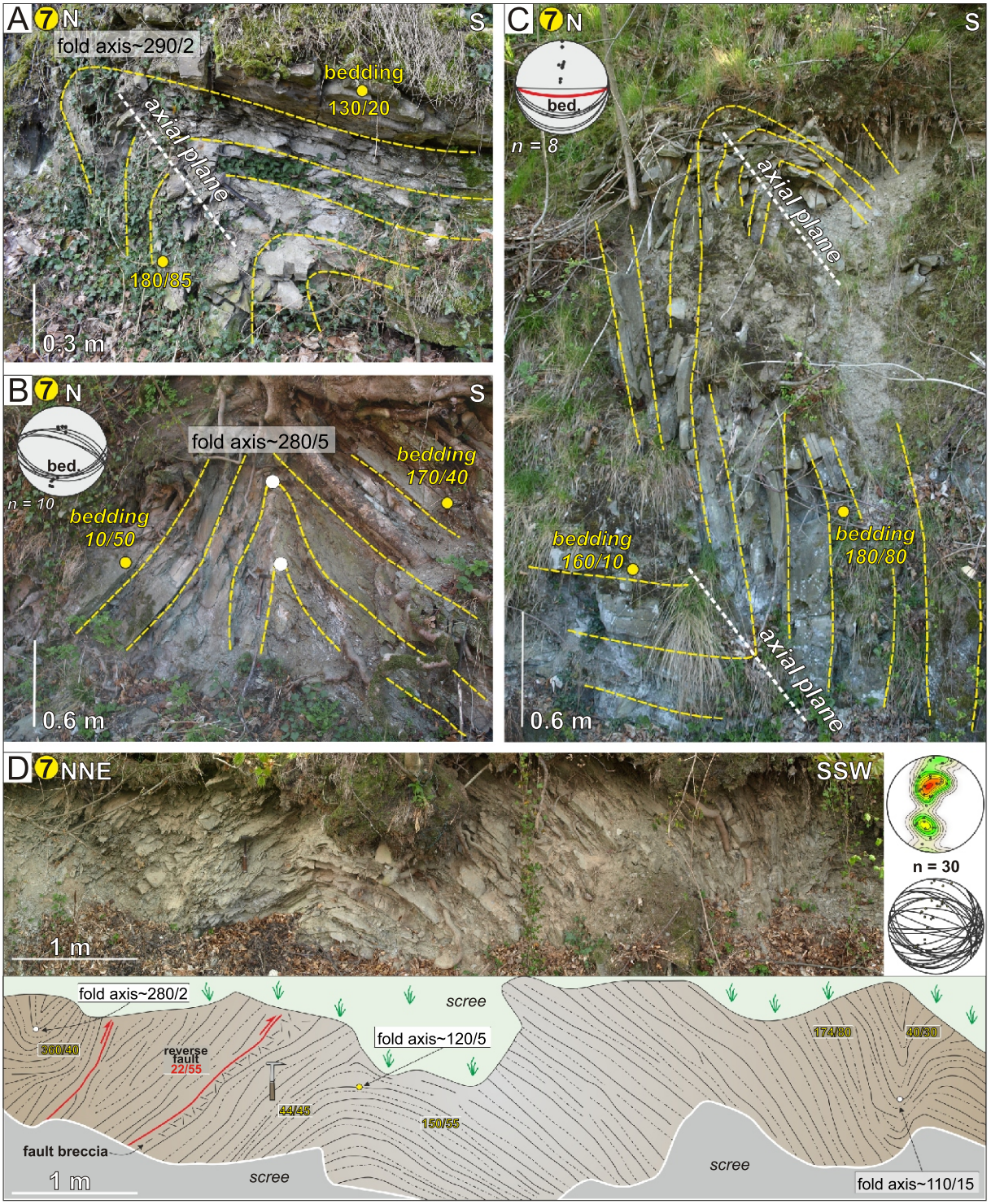

Fig. 7. Exposure-scale folds in Carboniferous sandstones in the southernmost part of the Kamionki Graben (loc. 7)

The bedding attitudes (shown as yellow dashed lines) are described with dip direction/dip angle. Inset stereoplots are lower hemisphere, equal area projections on a Schmidt-Lambert net showing bedding orientation (bed). **A** – an asymmetrical, N-vergent anticline (fault-propagation fold) developed in the hanging wall of a thrust fault. Sandstone beds show evidence of dragging above the fault (located mostly below the exposure bottom); **B** – upright, tight, nearly symmetrical anticline with chevron profile, vertical axial plane and horizontal hinge line; **C** – inclined, asymmetrical folds with axial plane dipping nearly 60° to the S (red great circle) affecting sandstone beds; **D** – open to tight, E–W to WNW–ESE-trending folds, cut by two minor reverse faults in the NNE part of the stream valley profile

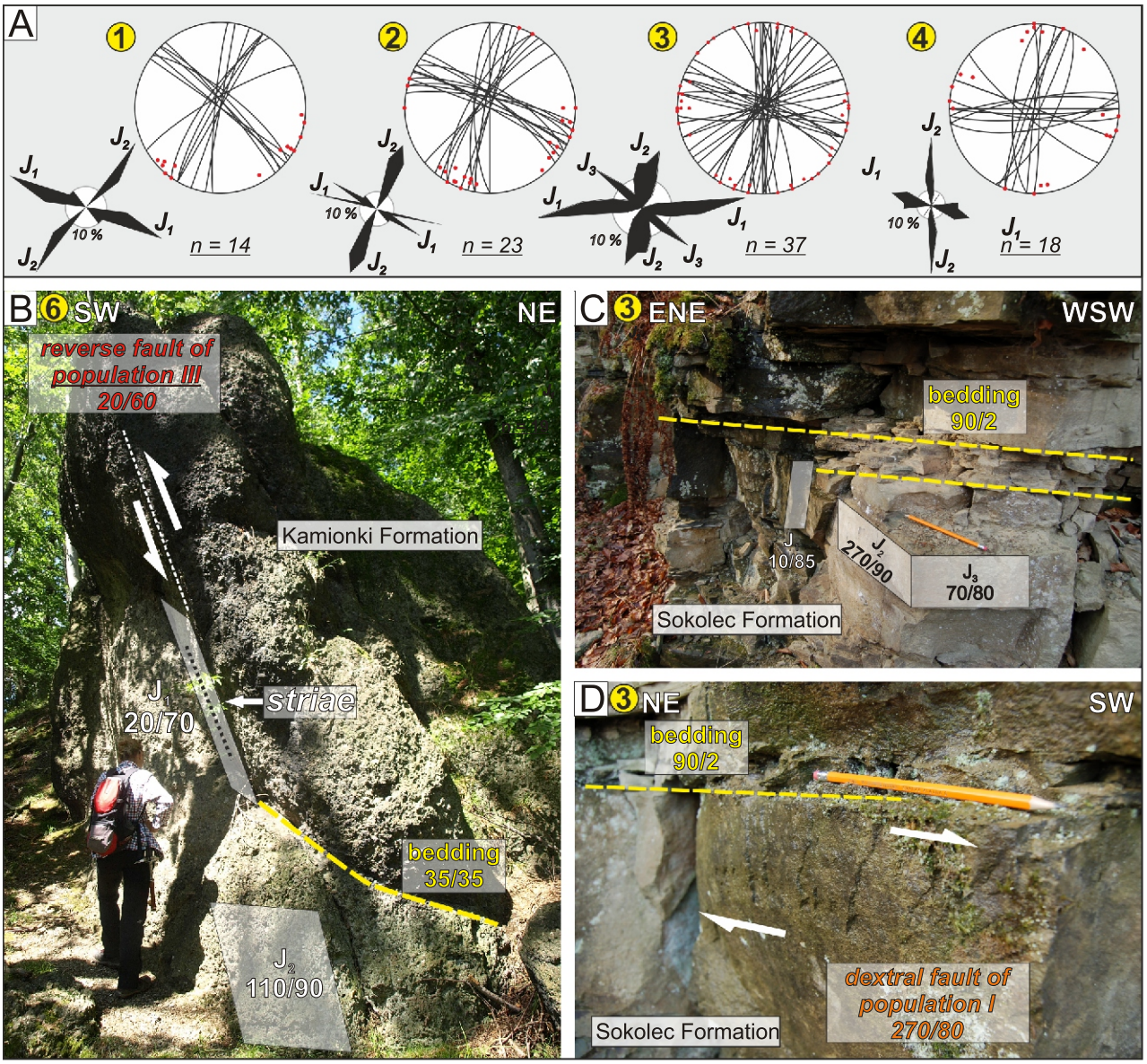

Fig. 8. Joints, faults and related structures in the Carboniferous succession of the Kamionki Graben. Numbers of exposures are indicated in yellow circles (see Fig. 2 for the locations)

Orientation of joints is shown as rose diagrams (circular frequency polygon plots) and as stereoplots (lower hemisphere, equal area projections on a Schmidt-Lambert net). **A** – joint systems in Carboniferous conglomerates (loc. 1, 2 and 4) and sandstones (loc. 3); **B** – two sets of joints cutting conglomerates in a tor near the eastern margin of the graben (loc. 6). Planar surface of reverse fault of population III related to J_1 joint is marked; **C** – three sets of planar, vertical to subvertical bed-confined fractures cutting nearly horizontal sandstones exposed in an abandoned quarry near the western margin of the graben on the footwall of the Western Kamionki Fault (loc. 3); **D** – surface of J_2 joint in sandstone, showing evidence of shearing in a dextral strike-slip regime (loc. 3); plane of a population I dextral fault

NE–SW trending, sets of fractures were also observed within folded sandstones and mudstones in the southernmost portion of the graben (loc.7).

Four genetically different sets of faults with a constrained slip sense, referred to here as populations numbered I–IV, have been recognized and measured within the KG and within its metamorphic basement (Figs. 8D and 9). Populations I–IV were separated into homogeneous sets based on kinematic criteria and cross-cutting relationships.

Population I consists of steep strike-slip dextral faults with non-planar/curved surfaces, which are dissecting sandstones exposed along the Western Kamionki Fault (loc. 3). They are oriented subparallel to the trough elongation and reveal dips greater than ~70°. Most of these faults represent reactivated (predominantly in a dextral strike-slip regime) planar non-striated joint surfaces trending N-S to NNW-SSE, both assigned to the J_2 joint set (Fig. 8D). A few dextral faults were also observed within nearly vertically-dipping sandstones near the Western

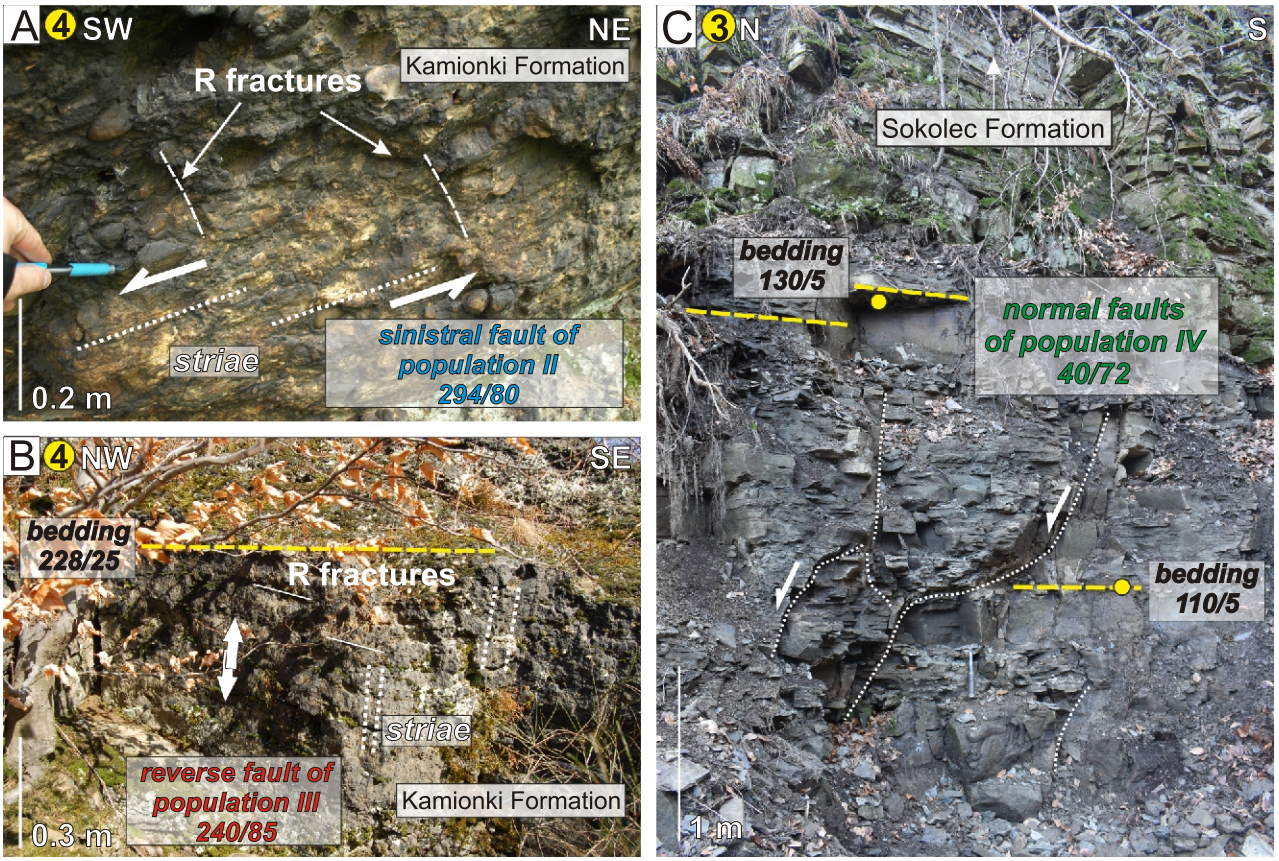

Fig. 9. Examples of faults of populations II–IV in the Carboniferous succession of the Kamionki Graben

Numbers of exposures are indicated in yellow circles (see Fig. 2 for the locations). **A** – polished and striated plane of a population II sinistral fault accompanied by R fractures; **B** – polished and striated surface of a population III reverse fault; the fault is oriented sub-parallel to the Eastern Kamionki Fault; **C** – non-planar faults of population IV (normal) faults exposed near the Western Kamionki Fault

Kamionki Fault. The orientation of compression (P) calculated for the faults of population I vary between ~15.2–195.2 and ~44.2–224.2° (mean: 35.0°; Table 1).

Population II includes the steeply inclined, NNW-SSE to NNE–SSW-striking, sinistral faults recorded in the Carboniferous conglomerates (loc. 4; Fig. 9A) and in gneisses exposed along the Western Boundary Fault, near the southern corner of the graben (loc. 8). At loc. 4, NNW–SSE to NNE–SSW-trending sinistral faults occur with well-developed horizontal or subhorizontal slickensides, asymmetrical ridges, and steps (Fig. 9A). They are sub-parallel to the strike of the Pniaki Fault (Fig. 2). The reconstructed shortening (P) axes calculated from fault-slip data of this population vary between ~109.9–289.9° and 155.2–335.2° (WNW–ESE to NW–SE-oriented, nearly horizontal compression and ENE–WSW to NE–SW-oriented extension) in the Carboniferous conglomerates to ~105.2–285.2 and 134.9–314.9 in the gneisses (NW–SE- and WNW–ESE oriented nearly horizontal compression) and imply a sinistral component of motion (Table 1).

The faults of population III were observed to occur within the polymictic conglomerates exposed locally near the northern margin of the Kamionki Graben (loc. 4; Fig. 9B). The conglomerates host steep, NW–SE-striking minor faults, parallel and sub-parallel to the map-scale fold axes and the graben's boundary faults. The fault surfaces display well-developed slickensides, asymmetrical ridges and steps indicating the reverse sense of displacements (Fig. 9B). At loc. 4, faults of this population are represented by steep, striated surfaces with dip angles ranging ~75–80° towards the NE and strike lines oriented obliquely to the Pniaki Fault. These faults cut older, population II sinistral faults. A conjugate system of reverse faults with dips at ~60–75°, both towards the NNE and SSW, is exposed also at loc. 6. The fault lines are oriented parallel and sub-parallel to the Middle Kamionki Fault. The reverse faults of population I reveal WSW–ENE to NE–SW subhorizontal compression (P) direction of ~11.7–191.7 and ~73.3–253.3° (mean: 66.9°) and WNW–ESE to NW–SE steeply inclined extension (T) axes (Table 1 and Fig. 10).

The faults of population IV were observed in sandstones exposed along the Western Kamionki Fault (loc. 3; Fig. 9C). They are oriented subparallel to the graben elongation and reveal dips greater than ~70°. These faults represent planar or curved discontinuities trending NW–SE, with little evidence of displacements (Fig. 9C). The orientation of extension (T) direction calculated for the faults of population IV vary between ~24.0–35.0 and ~230.0° (mean: 34.2°) with a nearly subvertical, NE–SW directed mean compression (P) direction of ~214.1/65.6 (Table 1 and Fig. 10).

Table 1

Selected parameters, measured orientations and principal axes of the finite strain ellipsoid of individual faults in the Kamionki Graben area

Id.	S. no.	Lit.	Sl.	Fault pop.	Fault plane		Striae		P axis		T axis		B axis	
					strike	dip	trend	plunge	trend	plunge	trend	plunge	trend	plunge
1	2	St	R	I	180	80	359	5	44.2	10.5	134.9	3.6	243.6	78.9
2	2	St	R	I	360	90	180	0	45.0	0.0	135.0	0.0	90.0	90.0
3	2	St	R	I	185	85	185	0	49.9	3.2	140.1	3.8	280.0	85.0
4	2	St	R	I	330	65	333	6	193.7	13.3	289.1	21.5	74.2	64.3
5	2	St	R	I	330	85	330	5	195.2	0.0	285.2	7.1	105.0	82.9
6	2	St	N	IV	310	72	40	72	220.0	63.0	24.0	40.0	310.0	0.0
7	2	St	N	IV	305	60	35	60	215.0	75.0	35.0	15.0	305.0	0.0
8	2	St	N	IV	305	75	35	75	215.0	60.0	35.0	30.0	305.0	0.0
9	2	St	N	IV	140	50	230	50	50.0	85.0	230.0	05.0	320.0	0.0
10	4	Cg	T	III	330	80	60	80	60.0	35.0	240.0	55.0	330.0	0.0
11	4	Cg	T	III	345	75	67	75	73.3	30.0	258.0	59.9	164.4	2.1
12	4	Cg	T	III	340	80	65	80	69.3	35.0	251.1	55.0	159.8	0.9
13	4	Cg	T	III	335	80	60	80	64.3	35.0	246.1	55.0	154.8	0.9
14	4	Cg	L	II	340	90	160	6	114.9	4.0	205.1	4.0	340.0	84.3
15	4	Cg	L	II	335	90	155	5	109.9	3.8	200.1	3.8	335.0	84.7
16	4	Cg	L	II	200	85	201	9	155.2	9.8	245.6	2.7	350.7	79.9
17	4	Cg	L	II	185	70	189	10	143.3	21.7	50.7	6.5	304.8	67.2
18	4	Cg	L	II	160	85	161	15	114.8	14.1	206.5	6.9	321.9	74.3
19	4	Cg	L	II	345	90	165	6	119.8	4.2	210.2	4.2	345.0	84.0
20	4	Cg	L	II	180	70	184	10	138.3	21.7	45.7	6.5	299.8	67.2
21	4	Cg	L	II	165	80	167	11	120.9	14.6	211.0	0.4	302.5	75.4
22	6	Cg	T	III	110	60	200	60	200.0	15.0	20.0	75.0	290.0	0.0
23	6	Cg	T	III	290	60	47	57	30.5	13.8	166.8	71.2	297.4	12.5
24	6	Cg	T	III	306	60	36	60	36.0	15.0	216.0	75.0	306.0	0.0
25	6	Cg	T	III	280	70	16	70	11.7	25.0	186.5	64.9	280.7	2.0
26	6	Cg	T	III	110	75	200	75	200.0	30.0	20.0	60.0	290.0	0.0
27	8	Gn	L	II	180	80	359	5	134.9	3.6	44.2	10.5	243.6	78.9
28	8	Gn	L	II	360	90	0	0	135.0	0.0	45.0	0.0	90.0	90.0
29	8	Gn	L	II	185	85	185	0	140.1	3.8	49.9	3.2	280.0	85.0
31	8	Gn	L	II	330	65	333	6	289.1	21.5	193.7	13.3	74.2	64.3
32	8	Gn	L	II	330	85	330	5	285.2	7.1	195.2	0.0	105.0	82.9

S – measurement site; Lit – lithology: St – sandstone, Cg – conglomerate, Gn – gneiss; Sl – sense of slip: R – dextral, L – sinistral, N – normal, T – thrust/reverse fault; Fault pop. – fault population distinguished

INTERPRETATION AND DISCUSSION: STRUCTURAL EVOLUTION OF THE KAMIONKI GRABEN

Due to the very limited number of exposures, sparse fault-slip data and the lack of a clear Meso-Cenozoic geological record in the uplifted area of the Góry Sowie Block, a precise reconstruction of its structural evolution faces considerable difficulties. Nevertheless, the evolution of the KG developed on top of the GSM can be roughly reconstructed, using the criteria of the superposition and relationships between the ductile and brittle tectonic deformation structures. Palaeostress data from adjacent geological units, exposing younger, slightly deformed lower Permian to Upper Cretaceous strata, may also be useful in this task. Based on the results of geological mapping, structural analysis and geophysical survey, the interpretation proposed here assumes a relatively complex, polyphase (at least four-stage) development of the Kamionki Graben area, that began in the Carboniferous and lasted until the late Cenozoic (Fig. 11).

The Carboniferous succession of the Góry Sowie Massif was folded (and, locally, also probably thrusted over the gneissic basement) into the ESE–WNW to E–W and, less frequently, NW–SE oriented folds at the end of the Mississippian (Namurian ?) epoch (Fig. 11). The fold axes measured are nearly perpendicular to the direction of the interpreted NNE-SSW to N-S horizontal compression at the NE foreland of the Bohemian Massif during the end-Variscan orogeny (Edel et al., 2018; Mazur et al., 2020). Fold structures of similar geometry are widespread in the Carboniferous strata deposited in the system of late-orogenic, collision-related, foreland- and intra-montane basins that developed at the NE and E margins of the Bohemian Massif (e.g., Hartley and Otava, 2001; Bábek et al., 2004; Narkiewicz, 2007; Mazur et al., 2010; Narkiewicz, 2020). Late Paleozoic, dextral movements along the main crustal shear zone faults of the NE Bohemian Massif that acted during the final pulses of the Variscan orogeny have been postulated and documented by many authors (e.g., Aleksandrowski et al., 1997; Edel et al., 2018; Žák et al., 2018; Mazur et al., 2020). The dextral displacements were probably related to

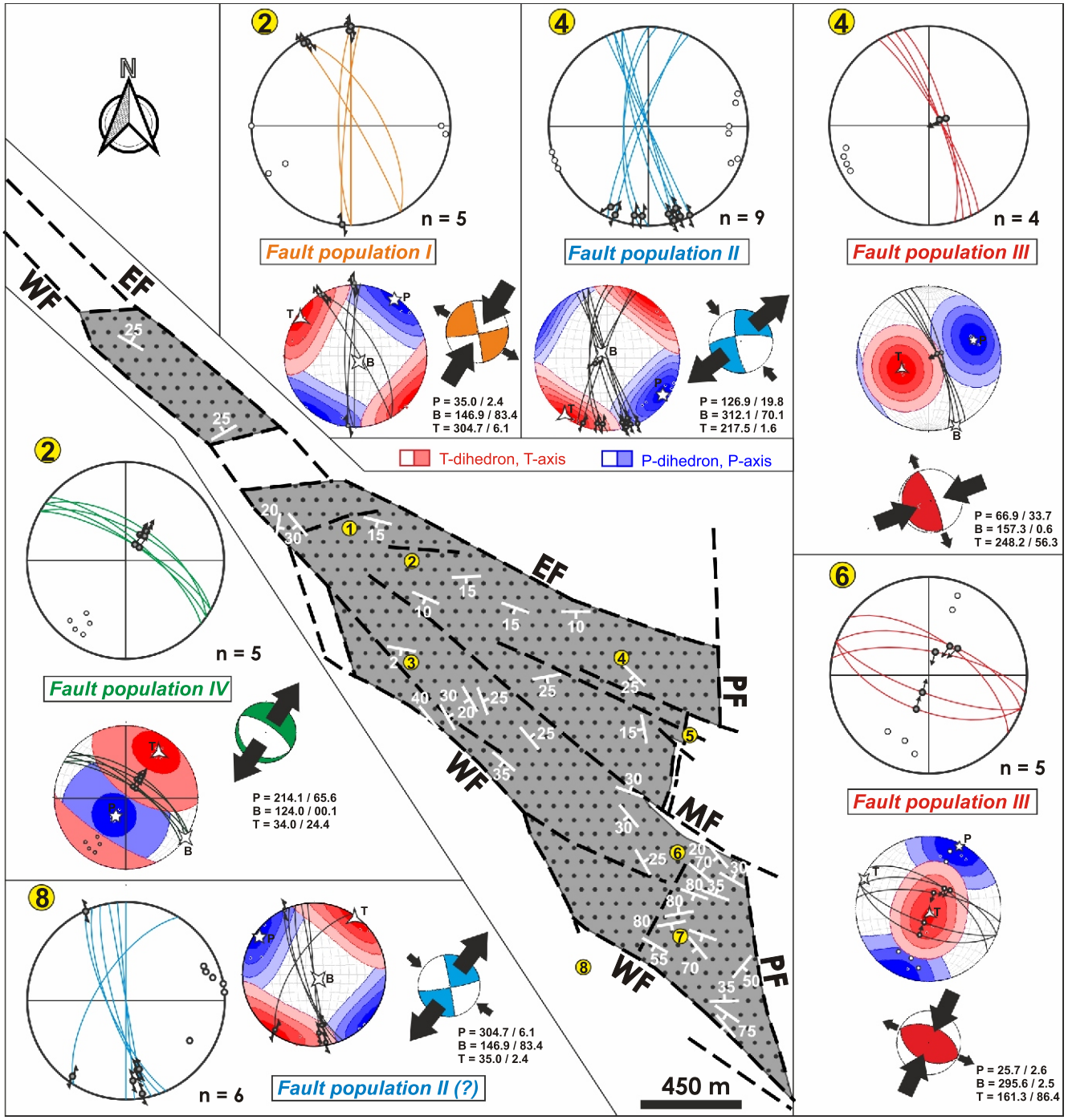

Fig. 10. Kinematic data collected on minor faults and interpretation of the principal axes of finite strain ellipsoids calculated using the PBT method – moment tensor analysis (Angelier 1984; Marrett and Allmendinger 1990; Pascal 2021) for the four homogenous fault systems (populations) I–IV distinguished in the Kamionki Graben

The fault plane orientations collected are shown on the great circle diagrams with marked poles. Striae on fault planes are shown as dots with arrows indicating the sense of displacement of the hanging wall block. The inset "beachball plots" obtained from moment tensor analysis show shortening (P) and extension (T) quadrants. Numbers of exposures are indicated in yellow circles

the motion (oblique convergence) between Gondwana-derived microcontinents and the continent of Laurussia (Hofmann et al., 2009; Martínez Catalán, 2012, 2021; Franke et al., 2017; Edel et al., 2018; Žák et al., 2018; Tomek et al., 2019). The mesoscale folds attributed to this regional shortening event are the most common structures in the southernmost portion of the Kamionki Graben between its boundary faults. The average shortening (P) axis orientation obtained from the dextral faults (referred to as fault population I; Fig. 10) in the Kamionki Graben reflects a similar, overall NNE–SSW to NE–SW compression direction (Fig. 10). Therefore, it cannot not be excluded that the transpression generated by the strike-slip dextral displacements may have played an active role in the folding process.

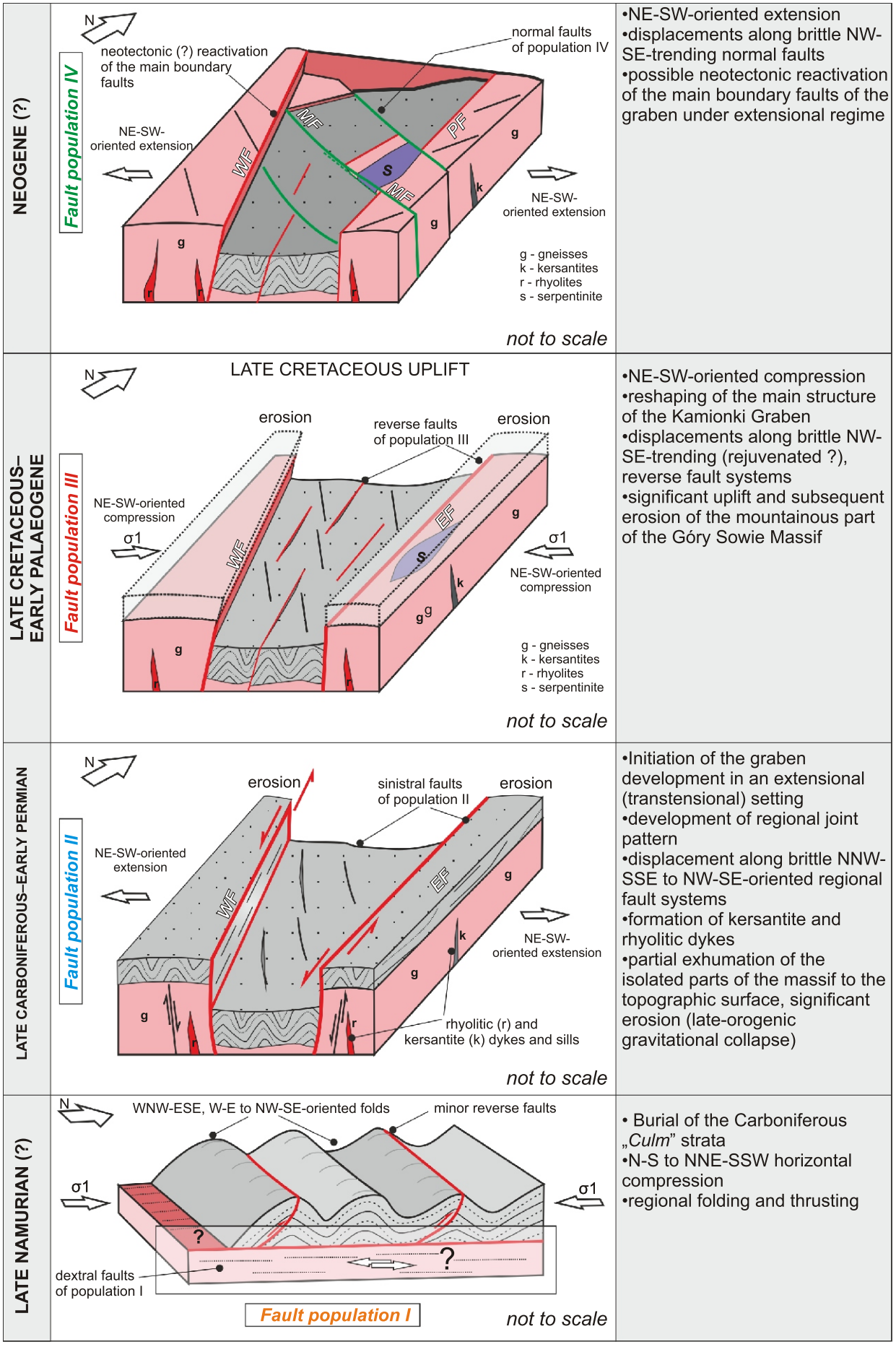

Fig. 11. Schematic model showing evolution of the Kamionki Graben

For further explanations see the text

The formation of the Kamionki Graben as a tectonic depression included displacements along NNW–SSE to NW–SE striking high-angle faults (Fig. 11). These occurred over a long period between the Namurian (late Mississippian) and Neogene, starting some time between the late Carboniferous and early Permian. The development of the graben must have occurred only slightly after the folding of the Carboniferous succession and is correlated by the authors with a significant, late Carboniferous to early Permian regional uplift and erosion, associated with the gravitational collapse of the newly formed Variscan orogen (e.g., Mazur et al., 2006; Žák et al., 2018). Various parts of the GSM were then progressively exhumed and supplied gneissic detritus to the nearby Intra-Sudetic Basin (Mastalerz, 1996). However, Aramowicz et al. (2006), postulated, on the basis of apatite fission-track dating (AFT), that the shoulders of the Kamionki Graben, together with the entire Góry Sowie Block, were probably partly covered by Carboniferous and Permian sediments during late Carboniferous and Permian times. These results suggest a significant episode of burial under a thick cover of Paleozoic clastic deposits.

Based on the above, we interpret the NNW–SSE to NNE–SSW striking, strike-slip (mainly sinistral) faults of population II (Fig. 10) as the result of NE–SW to WNW–ESE regional extension (transtension) in late Carboniferous to early Permian times (Fig. 11). These faults must have been reactivated during the latest, successive tectonic events affecting the Carboniferous succession preserved on top of the Góry Sowie Massif (Fig. 11). Sinistral movement along the nearby Intra-Sudetic (Głuszyca) Fault, striking parallel to the Kamionki Graben, between the late Carboniferous and early Permian, has been postulated by Aleksandrowski et al. (1997). The inferred late Carboniferous–early Permian extensional stage coincides with the widespread subsidence event associated with the initial stages of the Polish Basin's development (Krzywiec et al., 2022). The formation of kersantite and rhyolite dykes, which predominantly trend NW–SE to NNW–SSE and are exposed in the Góry Sowie Massif area (Grocholski, 1967; Awdankiewicz, 2007), as well as the emplacement of volcanic and sub-volcanic bodies in the adjacent Intra-Sudetic Basin (Awdankiewicz, 1999, 2022), appear to be genetically linked to this evolutionary stage.

Reconstructing the structural evolution of the Góry Sowie Massif and interpreting the tectonic events spanning from the Early Triassic to the Late Cretaceous is exceedingly challenging. A sedimentary cover of Early Triassic and possibly even Jurassic age may have once existed in the study area, although its extent remains undetermined. Lower Triassic deposits are preserved in the nearby Intra-Sudetic and North-Sudetic basins (e.g., Mroczkowski and Mader, 1985). Petrographic analyses of these deposits, however, suggest that the Góry Sowie Massif may have served as a source area for these basins during the Triassic (Mroczkowski, 1969; Mroczkowski and Mader, 1985; Kowalski, 2020). Moreover, present-day outcrops of shallow-marine Jurassic deposits in the NE Bohemian Massif are confined to the Elbe Fault Zone (see Fig. 1A for location) (Valečka, 2019; Nádaskay et al., 2024). The original extent of these strata to the NE of this zone remains undetermined and continues to be a subject of ongoing discussion in the literature (Voigt, 2009; Hofmann et al., 2018; Nádaskay et al., 2019, 2024; Valečka, 2019). Nadaskay et al. (2019), using heavy mineral assemblages and U-Pb detrital zircon geochronology, interpreted substantial extensional reactivation of major Variscan faults in the NE Bohemian Massif during the Middle–Late Jurassic as well as in the Early Cretaceous. These postulated extensional phases coincide with pulses of extension-related subsidence in the Polish Basin during the Late Jurassic and early Cenomanian (Dadlez et al., 1995; Stephenson et al., 2003). The possible reactivation of NW–SE-trending faults in the NE Bohemian Massif is thought to have led to enhanced subsidence northeast of the Elbe Fault Zone and an increase in sediment supply to the area of the present-day Lusatian Massif during the Middle Jurassic to Early Cretaceous. However, in their palaeogeographic reconstructions, Nádaskay et al. (2019) depicted the Góry Sowie Block as lacking Jurassic and Cretaceous cover during this period. Thus, the extent of the Jurassic deposits – and whether they covered the Sudetes region – remains unresolved. It is widely accepted that, during the Late Cretaceous, the Góry Sowie Massif acted as a source area for the Intra-Sudetic and North-Sudetic basins, representing an emerged segment of the Eastern Sudetic Island that supplied clastic sediment to these basins (e.g., Voigt, 2009; Biernacka, 2012; Leszczyński and Nemec, 2020; Kowalski, 2021a, b).

The Late Cretaceous–early Paleogene uplift of the Góry Sowie Massif along the Sudetic Marginal and Głuszyca faults to the NE and SW, respectively, must have resulted in subsequent erosion of the mountainous part of the massif (Fig. 11). The uplift was due to Late Cretaceous–early Paleogene, regional, NE–SW-oriented tectonic compression and concomitant inversion, which affected the western and central European Alpine foreland (Rosenbaum et al., 2002; Mazur et al., 2005; Kley and Voigt, 2008; Voigt et al., 2021; Głuszyński and Aleksandrowski, 2022). An average orientation of shortening (P) axis calculated from fault population III (Fig. 10) corresponds to the regionally reported palaeostress and regional-tectonic data documenting this Late Cretaceous–early Cenozoic deformation of the NE fringe of the Bohemian Massif (Pešková et al., 2010; Coubal et al., 2015; Novakova, 2015; Kowalski, 2021a, b; Sobczyk and Szczygieł, 2021; Głuszyński and Aleksandrowski, 2022). A relatively uniform, NE–SW to ENE-WSW oriented compressional stress regime is interpreted as a result of far-field effects of the Europe-Iberia-Africa plate convergence at ~86–70 Ma (Rosenbaum et al., 2002; Kley and Voigt, 2008). A broad range of similarly oriented, inversion structures (both brittle and ductile) related to this deformation event is commonly observed throughout Central Europe in the foreland of the Alpine-Carpathian deformation front (Kozdrój and Cymerman, 2003; Mazur et al., 2005; Kley and Voigt, 2008; Krzywiec et al., 2018, 2022; Voigt et al., 2021; Głuszyński and Aleksandrowski, 2022). These structures include low- to high-angle reverse and normal faults, thrusts delimiting basement highs, inverted basins and grabens, as well as marginal troughs (Voigt et al., 2021). The total amount of denudation of the Góry Sowie Massif linked with this tectonic event is estimated at 4–8 km (Aramowicz et al., 2006) and at least 4 km for the adjacent Intra-Sudetic Basin (Botor et al., 2019). Based on the apatite fission track (AFT) data and thermal modelling results, Danišik et al. (2012) argued that the reverse faults and low-angle thrusts were active in the Sudetic region between 85–70 Ma.

Normal faults of population IV (Figs. 9C and 10), oriented nearly parallel to the graben elongation, are likely associated with the most recent stage of the brittle deformation linked to the NE–SW-oriented extensional regime. These faults are parallel to the strike lines of the NW–SE oriented faults that displace sedimentary rocks within the KG. This stress orientation can be correlated with the youngest brittle deformation structures revealed by fault-slip data and recorded in the vicinity of the Sudetic Marginal Fault (Krzyszkowski and Pijet, 1993; Krzyszkowski and Olejnik, 1998; Różycka et al., 2021; Migoń et al., 2023). Sub-recent neotectonic transformation of the pre-existing faults cannot be excluded in the study area. Neotectonic, extensional fault reactivation may have influenced the forma-

tion of the present-day valley network, especially of the Kamionka river valley. The rectilinear course of this valley may be explained by such fault activity.

Another important issue is the origin of the systematic joints in the sedimentary rocks studied. The WNW–ESE to NW–SE and NE–SW trending joint sets, similar to those in the grabens on top of the GSM, were also observed within the Permo-Mesozoic rocks exposed in the nearby Intra-Sudetic and North-Sudetic synclinoria (Jerzykiewicz, 1968; Solecki, 1994). Although these latter joint sets are interpreted as Late Cretaceous–early Paleogene in age (Jerzykiewicz, 1968; Solecki, 2011; Głuszyński and Aleksandrowski, 2022), it cannot be excluded that in the study area the initiation and development of the joint pattern was linked with a stress field that was present during the waning stages of the Variscan orogeny. Such late Variscan joints were eventually rotated during successive phases of brittle and ductile deformation. Due to the limited number of exposures in the Kamionki Graben area this issue requires systematic research in the future, also in the areas of adjacent tectonic units composed mainly of strongly folded Carboniferous sedimentary strata (i.e. the Świebodzice Depression and the Bardo Structure; cf. Oberc 1972; Wajsprych, 1978; Porębski, 1990).

SUMMARY AND CONCLUSION

The Kamionki Graben constitutes a distinct, fault-bounded tectonic feature superimposed on the crystalline basement of the metamorphic Góry Sowie Massif and filled with deformed, syn- to late-orogenic Mississippian ("Culm") sedimentary rocks. The results of our geological mapping, structural analysis and geophysical survey, integrated with available regional palaeostress data, point to an at least four-stage evolution of the Kamionki Graben area in Carboniferous to Cenozoic times. This study shows that the Carboniferous succession on top of the Góry Sowie Massif was folded (and possibly thrusted over the gneissic basement) probably at the end of the Namurian. The trends of the dominant NW–SE- and minor E–W-oriented folds are nearly perpendicular to the direction of the pronounced NE–SW to N–S direction of horizontal compression attributed to the end of the Variscan orogeny. The average shortening axis orientation obtained from dextral faults of fault population I in the Kamionki Graben reflects a similar, overall NNE–SSW to NE–SW compression direction. Hence, it cannot not be excluded that the transpression generated by the strike-slip dextral displacements may have played an active role in the folding process of the Carboniferous strata.

The brittle deformation structures in the Mississippian strata of the Kamionki Graben are predominantly late- to post-Carboniferous (early Permian?) and are interpreted here as younger than the folds. The authors interpret the marginal faults of the graben as genetically linked to a late Carboniferous–early Permian extension (transtension) phase, which contributed to the development of the graben and its boundary faults. Probable Early Triassic–Early Cretaceous (?) extension further accentuated this process, preserving the Carboniferous deposits within the graben until later denudation. The evidence for these tectonic events must have been partially overprinted during the younger stages of the graben development. The true amount of vertical and horizontal displacements along the marginal faults of the graben cannot be reliably assessed; it may reach a few hundred or even thousands of metres.

The marginal and internal faults of the graben have recorded reverse displacements as well as the youngest – normal – displacements.The reverse faults are interpreted as resulting from the NE–SW-oriented dominant compression related to the widespread Late Cretaceous–early Paleogene inversion event which affected the western-central European foreland. The NE–SW-oriented regional compression was linked to far-field effects of the Europe-Iberia-Africa plate convergence at ~86–70 Ma. The NW–SE-striking reverse faults that formed during this tectonic event may represent older, rejuvenated discontinuities, primarily originated during the Variscan orogeny. The still younger generations of normal faults provide evidence for extensional movements. A contemporaneous (neotectonic), possibly extensional, transformation of the pre-existing faults in the Kamionki Graben cannot be ruled out.

Our study provides the first detailed documentation of the structure and interpreted kinematics of the Kamionki Graben. Strong lithological contrasts between the sedimentary infill of the graben and its crystalline shoulders and floor, makes seismic and resistivity geophysical methods a valuable tool for investigation of the graben internal structure. The results presented in this paper can be useful in the context of discussions on the deformation style and stress field recostructions at the front of the Variscan and Alpine orogens in Central Europe during the Carboniferous and Late Cretaceous–early Paleogene. Our interpretations contribute to understanding of the post-Variscan evolution of the NE Bohemian Massif.

Acknowledgements. The research was a part of the statutory project no. 61.2608.2400.00.0 of the Polish Geological Institute – National Research Institute. The results of geological mapping and 2D Electrical Resistivity Tomography (ERT) and 2D Seismic P-wave Refraction Tomography (SRT) presented in the paper was funded by the Ministry of the Climate and Environment of Poland from the sources of the National Fund for Environment Protection and Water Management (project no 22.0201.1901.01.1: "Prace kartograficzne na 3 arkuszach Szczegółowej Mapy Geologicznej Sudetów 1:25 000: Zagórze Śląskie, Pieszyce, Ostroszowice – etap I"). We are grateful to two anonymous reviewers for their extensive comments and insightful suggestions, which significantly improved the quality of our manuscript. We extend our sincere thanks to Krzysztof Mastalerz, Paweł Aleksandrowski, Jacek Szczepański, and Marcin Dąbrowski for their thorough early reviews and numerous suggestions. Special thanks also go to Roland Nádaskay for his valuable comments on the region's geology. We also thank Jan Zalasiewicz for his linguistic corrections to the paper.

REFERENCES

ABEM, 2011. Terraloc Pro. Instruction Manual. Available online: https://wwwguidelinegeoc.cdn.triggerfish.cloud/uploads/2016/03/Terraloc-Pro-Instruction-Manual.pdf (accessed on 10 July 2022)

ABEM, 2012. Terrameter, L. Instruction Manual, Edited. Available online: https://wwwguidelinegeoc.cdn.triggerfish.cloud/uploads/2016/03/User-Guide-Terrameter-LS-2012-10-25.pdf (accessed on 5 May 2023)

Aleksandrowski, P., Kryza, R., Mazur, S., Żaba, J., 1997. Kinematic data on major Variscan strike-slip faults and shear zones in the Polish Sudetes, northeast Bohemian Massif. Geological Magazine, **133**: 727–739; https://doi.org/10.1017/S0016756897007590

Aleksandrowski, P., Kryza, R., Mazur, S., Pin, C., Zalasiewicz, J.A., 1999. The Polish Sudetes: Caledonian or Variscan? Transactions of the Royal Society of Edinburgh: Earth Sciences, **90**: 127–146; https://doi.org/10.1017/S0263593300007197

Angelier, J., 1984. Tectonic analysis of fault slip data sets. Journal of Geophysical Research: Solid Earth, **89**: 5835–5848; https://doi.org/10.1029/JB089iB07p05835

Aramowicz, A., Anczkiewicz, A., Mazur, S., 2006. Fission-track dating of apatite from the Góry Sowie Massif, Polish Sudetes, NE Bohemian Massif: implications of post-Variscan denudation and uplift. Neues Jahrbuch für Mineralogie Abhandlungen, **182**: 221–229; https://doi.org/10.1127/0077-7757/2006/0046

Augustyniak, K., Grocholski, A., 1968. Geological structure and outline of the development of the Intra-Sudetic depression. Biuletyn Instytutu Geologicznego, **17**: 87–111.

Awdankiewicz, M., 1999. Volcanism in a late Variscan intramontane trough: Carboniferous and Permian volcanic centres of the Intra-Sudetic Basin, SW Poland. Geologia Sudetica, **32**: 13–47.

Awdankiewicz, M., 2007. Late Palaeozoic lamprophyres and associated mafic subvolcanic rocks of the Sudetes (SW Poland): petrology, geochemistry and petrogenesis. Geologia Sudetica, **39**: 11–97.

Awdankiewicz, M., 2022. Polyphase Permo-Carboniferous magmatism adjacent to the Intra-Sudetic Fault: constraints from U-Pb SHRIMP zircon study of felsic subvolcanic intrusions in the Intra-Sudetic Basin, SW Poland. International Journal of Earth Sciences, **111**: 2199–2224; https://doi.org/10.1007/s00531-022-02232-y

Bábek, O., Mikuláš, R., Zapletal, J., Lehotský, T., 2004. Combined tectonic-sediment supply-driven cycles in a Lower Carboniferous deep-marine foreland basin, Moravice Formation, Czech Republic. International Journal of Earth Sciences, **93**: 241–261; https://doi.org/10.1007/s00531-004-0388-5

Biernacka, J., 2012. Provenance of Upper Cretaceous quartz-rich sandstones from the North Sudetic Synclinorium, SW Poland: constraints from detrital tourmaline. Geological Quarterly, **56** (2): 333–344; https://doi.org/10.7306/gq.1024

Botor, D., Anczkiewicz, A., Mazur, S., Siwecki, T., 2019. Post-Variscan thermal history of the Intra-Sudetic Basin (Sudetes, Bohemian Massif) based on apatite fission track analysis. International Journal of Earth Sciences, **108**: 2561–2576; https://doi.org/10.1007/s00531-019-01777-9

Bröcker, M., Żelaźniewicz, A., Enders, M., 1998. Rb-Sr and U-Pb geochronology of migmatitic gneisses from the Góry Sowie (West Sudetes, Poland): the importance of Mid-Late Devonian metamorphism. Journal of the Geological Society, **155**: 1025–1036; https://doi.org/10.1144/gsjgs.155.6.1025

Brueckner, H., Blusztajn, J., Bakun-Czubarow, N., 1996. Trace element and Sm-Nd 'age' zoning in garnets from peridotites of the Caledonian and Variscan Mountains and tectonic implications. Journal of Metamorphic Geology, **14**: 61–73; https://doi.org/10.1111/j.1525-1314.1996.00061.x

Caputo, R., Piscitelli, S., Oliveto, A., Rizzo, E., Lapenna, V., 2003. The use of electrical resistivity tomographies in active tectonics: examples from the Tyrnavos Basin, Greece. Journal of Geodynamics, **36**: 19–35; https://doi.org/10.1016/S0264-3707(03)00036-X

Compton, R.R., 1962. Manual of field geology. John Wiley & Sons Inc., New York, London.

Coubal, M., Málek, J., Adamovič, J., Štěpančíková, P., 2015. Late Cretaceous and Cenozoic dynamics of the Bohemian Massif inferred from the paleostress history of the Lusatian Fault Belt. Journal of Geodynamics, **87**: 26–49; https://doi.org/10.1016/j.jog.2015.02.006

Cymerman, Z., 1998. The Góry Sowie Terrane: a key to understanding the Palaeozoic evolution of the Sudetes area and beyond. Geological Quarterly, **42** (4): 379–400.

Dadlez, R., Narkiewicz, M., Stephenson, R.A., Visser, M.T.M., van Wees, J.-D., 1995. Tectonic evolution of the Mid-Polish Trough: modelling implications and significance for central European geology. Tectonophysics, **252**: 179–195; https://doi.org/10.1016/0040-1951(95)00104-2

Dahlin, T., Zhou, B., 2004. A numerical comparison of 2D resistivity imaging with 10 electrode arrays. Geophysical Prospecting, **52**: 379–398.

Danišik, M., Štěpančíková, P., Evans, N., 2012. Constraining long-term denudation and faulting history in intraplate regions by multisystem thermochronology: an example of the Sudetic Marginal Fault (Bohemian Massif, central Europe). Tectonics, **31**, 2003; https://doi.org/10.1029/2011TC003012

Dathe, E., 1902. Geologische Karte von Preußen und benachbarten Bundesstaaten 1:25 000. Blatt Langenbielau., Lieferung 115. Preußischen Geologischen Landesalstalt, Berlin.

Davis, J.C., Sampson, R.J., 1986. Statistics and Data Analysis in Geology. Wiley, New York.

Don, J., Żelaźniewicz, A., 1990. The Sudetes – boundaries, subdivision and tectonic position. Neues Jahrbuch für Geologie und Paläontologie Abhandlungen, **179**: 121–127.

Drahor, M.G., Berge, M.A., 2017. Integrated geophysical investigations in a fault zone located on southwestern part of İzmir city, Western Anatolia, Turkey. Journal of Applied Geophysics, **136**: 114–133; https://doi.org/10.1016/j.jappgeo.2016.10.021

Dziedzic, K., Teisseyre, A.K., 1990. The Hercynian molasse and younger deposits in the Intra-Sudetic Depression, SW Poland. Neues Jahrbuch für Geologie und Paläontologie Abhandlungen, **179**: 285–305.

Edel J. B., Schulmann K., Lexa O., Lardeaux J., 2018. Late Palaeozoic palaeomagnetic and tectonic constraints for amalgamation of Pangea supercontinent in the European Variscan belt. Earth-Science Reviews, **177**: 589–612; https://doi.org/10.1016/j.earscirev.2017.12.007

el Hameedy, M.A., Mabrouk, W.M., Dahroug, S., Youssef, M.S., Metwally, A.M., 2023. Role of Seismic Refraction Tomography (SRT) in bedrock mapping; case study from industrial zone, Ain-Sokhna area, Egypt. Contributions to Geophysics and Geodesy, **53**: 111–128; https://doi.org/10.31577/congeo.2023.53.2.2

Fischer, T., Štěpančíková, P., Karousová, M., Tábořík, P., Flechsig, C., Gaballah, M., 2012. Imaging the Mariánské Lázně Fault (Czech Republic) by 3-D ground-penetrating radar and electric resistivity tomography. Studia Geophysica et Geodaetica, **56**: 1019–1036.

Franke, W., Żelaźniewicz, A., 2023. Variscan evolution of the Bohemian Massif (Central Europe): Fiction, facts and problems. Gondwana Research, **124**: 351–377; https://doi.org/10.1016/j.gr.2023.06.012

Franke, W., Cocks, L.R.M., Torsvik, T.H., 2017. The Palaeozoic Variscan oceans revisited. Gondwana Research, **48**: 257–284; https://doi.org/10.1016/j.gr.2017.03.005

Gawroński, O., 1961. Szczegółowa Mapa Geologiczna Sudetów w skali 1:25 000, arkusz Pieszyce (in Polish). Wyd. Geol., Warszawa.

Głuszyński, A., Aleksandrowski, P., 2022. Late Cretaceous-Early Palaeogene inversion-related tectonic structures at the NE margin of the Bohemian Massif (SW Poland and northern Czechia). Solid Earth, **13**: 1219–1242; https://doi.org/10.5194/se-13-1219-2022

Grocholski, W., 1967. Structure of the Sowie Mts. (in Polish with English summary). Geologia Sudetica, **3**: 181–249.

Gunia, T., 1999. Microfossils from the high-grade metamorphic rocks in the Góry Sowie Mts. (Sudetes area) and their stratigraphical importance. Geological Quarterly, **43** (4): 519–536.

Hartley, A.J., Otava, J., 2001. Sediment provenance and dispersal in a deep marine foreland basin: the Lower Carboniferous Culm Basin, Czech Republic. Journal of the Geological Society, **158**: 137–150; https://doi.org/10.1144/jgs.158.1.137

Haydukiewicz, J., 1990. Stratigraphy of Paleozoic rocks of the Góry Bardzkie and some remarks on their sedimentation (Poland). Neues Jahrbuch für Geologie und Paläontologie Abhandlungen, **179**: 275–284.

Hofmann, M., Linnemann, U., Gerdes, A., Ullrich, B., Schauer, M., 2009. Timing of dextral strike-slip processes and basement exhumation in the Elbe Zone (Saxo-Thuringian Zone): the final pulse of the Variscan Orogeny in the Bohemian Massif constrained by LA-SF-ICP-MS U-Pb zircon data. Geological Society Special Publications, **327**: 197–214; https://doi.org/10.1144/SP327.10

Hofmann, M., Voigt, T., Bittner, L., Gärtner, A., Zieger, J., Linnemann, U., 2018. Reworked Middle Jurassic sandstones as a marker for Upper Cretaceous basin inversion in Central Europe-a case study for the U-Pb detrital zircon record of the Upper Cretaceous Schmilka section and their implication for the sedimentary cover of the Lausitz Block (Saxony, Germany). International Journal of Earth Sciences, **107**: 913–932; https://doi.org/10.1007/s00531-017-1552-z

Imposa, S., Guidi, G.D., Grassi, S., Scudero, S., Barreca, G., Patti, G., Boso, D., 2015. Applying geophysical techniques to investigate a segment of a creeping fault in the urban area of San Gregorio di Catania, southern flank of Mt. Etna (Sicily – Italy). Journal of Applied Geophysics, **123**: 153–163; https://doi.org/10.1016/j.jappgeo.2015.10.008

Jastrzębski, M., Budzyń, B., Żelaźniewicz, A., Konečný, P., Sláma, J., Kozub-Budzyń, G.A., Skrzypek, E., Jaźwa, A., 2021. Eo-Variscan metamorphism in the Bohemian Massif: Thermodynamic modelling and monazite geochronology of gneisses and granulites of the Góry Sowie Massif, SW Poland. Journal of Metamorphic Geology, **39**: 751–779; https://doi.org/10.1111/jmg.12589

Jerzykiewicz, T., 1968. Remarks on the origin and orientation of joints in the Upper Cretaceous rocks of the Intrasudetic Basin (in Polish with English summary). Geologia Sudetica, **4**: 465–478.

Keller, G.V., Frischknecht, F.C., 1966. Electrical Methods in Geophysical Prospecting. Elsevier Science & Technology.

Kley, J., Voigt, T., 2008. Late Cretaceous intraplate thrusting in central Europe: Effect of Africa-Iberia-Europe convergence, not Alpine collision. Geology, **36**: 839–842; https://doi.org/10.1130/G24930A.1

Kowalski, A., 2020. Triassic palaeogeography of NE Bohemian Massif based on sedimentological record in the Wleń Graben and the Krzeszów Brachysyncline (SW Poland). Annales Societatis Geologorum Poloniae, **90**: 125–148; https://doi.org/10.14241/asgp.2020.09

Kowalski, A., 2021a. Late Cretaceous palaeogeography of NE Bohemian Massif: diachronous sedimentary successions in the Wleń Graben and Krzeszów Brachysyncline (SW Poland). Annales Societatis Geologorum Poloniae, **91**: 1–36; https://doi.org/10.14241/asgp.2021.05

Kowalski, A., 2021b. Multistage structural evolution of the end-Cretaceous-Cenozoic Wleń Graben (the Sudetes, NE Bohemian Massif) – a contribution to the post-Variscan tectonic history of SW Poland. Annales Societatis Geologorum Poloniae, **91**: 37–66; https://doi.org/10.14241/asgp.2020.21

Kowalski, A., 2024. Late- to post-Variscan structural evolution of tectonic grabens on top of the Góry Sowie Massif. In: 20th Jubilee Meeting of the Central European Tectonic Studies Groups CETEG, Srebrna Góra, 24-27.04.2024, Poland (eds. R. Sikora, M. Olkowicz and M. Adamuszek): 153–182. Abstract Volume and Field Trips Guide; https://doi.org/10.7306/CETEG2024-2

Kozdrój, W., Cymerman, Z., 2003. Alpine tectonic inversion-principal mechanism of the Variscan basement uplift and exhumation in the Sudety Mts. Geolines, **16**: 59–60.

Kröner, A., Hegner, E., 1998. Geochemistry, single zircon ages and Sm-Nd systematics of granitoid rocks from the Góry Sowie (Owl Mts), Polish West Sudetes: evidence for early arc-related plutonism. Journal of the Geological Society, **155**: 711–724; https://doi.org/doi.org/10.1144/gsjgs.155.4.0711

Kryza, R., Fanning, C.M., 2007. Devonian deep-crustal metamorphism and exhumation in the Variscan Orogen: evidence from SHRIMP zircon ages from the HT-HP granulites and migmatites of the Góry Sowie (Polish Sudetes). Geodinamica Acta, **20**: 159–175; https://doi.org/10.3166/ga.20.159-175

Kryza, R., Mazur, S., Oberc-Dziedzic, T., 2004. The Sudetic geological mosaic: Insights into the root of the Variscan orogen. Przegląd Geologiczny, **52**: 761–773.

Krzyszkowski, D., Olejnik, W., 1998. The Quaternary evolution of landscape and neotectonics of the Sowie Mts. range, Sudeten, Southwestern Poland. Geologia Sudetica, **31**: 221–239.

Krzyszkowski, D., Pijet, E., 1993. Morphological effects of Pleistocene fault activity in the Sowie Mts., southwestern Poland. Zeitschrift für Geomorphologie, **94**: 243–259.

Krzywiec, P., Stachowska, A., Stypa, A., 2018. The only way is up-on Mesozoic uplifts and basin inversion events in SE Poland. Geological Society Special Publications, **469**: 33–57; https://doi.org/10.1144/SP469.14

Krzywiec, P., Kufrasa, M., Poprawa, P., Mazur, S., Koperska, M., Ślemp, P., 2022. Together but separate: decoupled Variscan (late Carboniferous) and Alpine (Late Cretaceous-Paleogene) inversion tectonics in NW Poland. Solid Earth, **13**: 639–658; https://doi.org/10.5194/se-13-639-2022

Lasocki M., Bąk T., Czarniak P., Pacanowski G., Ostrowski S., Sobótka P., 2021. Dokumentacja badań geofizycznych wykonania metodą tomografii elektrooporowej (ERT) i sejsmiki refrakcyjnej (SRT-P) w ramach reambulacji Szczegółowej Mapy Geologicznej Sudetów w skali 1: 25000, arkusz Pieszyce, PIG-PIB Warszawa (in Polish), Arch. CAG PIG, Warszawa, CBDG: 1698642.

Leszczyński, S., Nemec, W., 2020. Sedimentation in a synclinal shallow-marine embayment: Coniacian of the North Sudetic Synclinorium, SW Poland. The Depositional Record, **6**: 144–171; https://doi.org/10.1002/dep2.92

Loke, M.H., 2000. Electrical Imaging Syrveys for Environmental and Engineering Studies. A Practical Guide to 2-D and 3-D Surveys, Geotomo, Malaysia.

Loke, M.H., 2012. Tutorial: 2-D and 3-D Electrical Imaging Surveys.Geotomo Software, Malaysia; http://refhub.elsevier.com/S0926-9851(18)31023-1/rf0365

Loke, M.H., Barker, R.D., 1996. Rapid least-squares inversion of apparent resistivity pseudosections by a quasi-Newton method. Geophysical Prospecting, **44**: 131–152; https://doi.org/10.1111/j.1365-2478.1996.tb00142.x

Loke, M., Alfouzan, F.A., Nawawi, M., 2007. Optimisation of electrode arrays used in 2D resistivity imaging surveys. ASEG Extended Abstracts, **1**: 1–4; https://doi.org/10.1071/ASEG2007ab002

Łapot, W., 1986. Petrography of Carboniferous rocks from the Sowie Mts. (in Polish with English summary). Geologia Sudetica, **21**: 1–144.

Łapot, W., 1988. Petrography of the Sowie Mts. Kulm. Bulletin of the Polish Academy of Sciences. Earth Sciences, **36**: 183–195.

Marrett, R., Allmendinger, R.W., 1990. Kinematic analysis of fault-slip data. Journal of Structural Geology, **12**: 973–986; https://doi.org/10.1016/0191-8141(90)90093-E

Martínez Catalán, J.R., 2012. The Central Iberian arc, an orocline centered in the Iberian Massif and some implications for the Variscan belt. International Journal of Earth Sciences, **101**: 1299–1314; https://doi.org/10.1007/s00531-011-0715-6

Martínez-Catalán, J.R., Schulmann, K., Ghienne, J.-F., 2021. The Mid-Variscan Allochthon: keys from correlation, partial retrodeformation and plate-tectonic reconstruction to unlock the geometry of a non-cylindrical belt. Earth-Science Reviews, **220**, 103700; https://doi.org/10.1016/j.earscirev.2021.103700

Mastalerz, K., 1995. Deposits of high-density turbidity currents on fan-delta slopes: an example from the upper Visean Szczawno formation, Intrasudetic Basin, Poland. Sedimentary Geology, **98**: 121–146; https://doi.org/10.1016/0037-0738(95)00030-C

Mastalerz, K., 1996. Fluvial sedimentation of the coal-bearing Žacler Formation (Westphalian) in the Wałbrzych Basin, SW Poland (in Polish with English summary). Acta Universitatis Wratislaviensis, Prace Geologiczno-Mineralogiczne, **52**: 21–85.

Mazur, S., Scheck-Wenderoth, M., Krzywiec, P., 2005. Different modes of the Late Cretaceous-Early Tertiary inversion in the North German and Polish basins. International Journal of Earth Sciences, **94**: 782–798; https://doi.org/10.1007/s00531-005-0016-z

Mazur, S., Aleksandrowski, P., Kryza, R., Oberc-Dziedzic, T., 2006. The Variscan Orogen in Poland. Geological Quarterly, **50** (1): 89–118.

Mazur, S., Aleksandrowski, P., Turniak, K., Krzemiński, L., Mastalerz, K., Górecka-Nowak, A., Kurowski, L., Krzywiec, P., Żelaźniewicz, A., Fanning, M., 2010. Uplift and late orogenic deformation of the Central European Variscan belt as revealed by sediment provenance and structural record in the Carboniferous foreland basin of western Poland. International Journal of Earth Sciences, **99**: 47–64; https://doi.org/10.1007/s00531-008-0367-3

Mazur, S., Paweł, A., Gągała, Ł., Krzywiec, P., Żaba, J., Gaidzik, K., Sikora, R., 2020. Late Palaeozoic strike-slip tectonics versus oroclinal bending at the SW outskirts of Baltica: case of the Variscan belt's eastern end in Poland. International Journal of Earth Sciences, **109**: 1133–1160; https://doi.org/10.1007/s00531-019-01814-7

Migoń, P., Latocha-Wites, A., Jancewicz, K., 2023. Geomorphology of the Sowie Mountains (Sudetes, SW Poland) – landform patterns and anthropogenic impact. Geographia Polonica, **96**: 103–129; https://doi.org/10.7163/GPol.0248

Mojica, A., Pérez, T., Toral, J., Miranda, R., Franceschi, P., Calderón, C., Vergara, F., 2017. Shallow electrical resistivity imaging of the Limón fault, Chagres River Watershed, Panama Canal. Journal of Applied Geophysics, **138**: 135–142; https://doi.org/10.1016/j.jappgeo.2017.01.010

Mroczkowski, J., 1969. Palaeocurrents in the Lower Triassic Deposits of the southern part of the Northsudetic Basin. Bulletin de l'Académie Polonaise des Sciences, Serie des Sciences Geologiques et Geographiques, **17**: 167–172.

Mroczkowski, J., Mader, D., 1985. Sandy inland braidplain deposition with local aeolian sedimentation in the lower and middle parts of the Buntsandstein and sandy coastal braidplain deposition in the topmost Zechstein in the Sudetes (Lower Silesia, Poland). In: Aspects of Fluvial Sedimentation in the Lower Triassic Buntsandstein of Europe (ed. D. Mader): 165–195. Springer, Berlin.

Müller, K., Polom, U., Winsemann, J., Steffen, H., Tsukamoto, S., Günther, T., Igel, J., Spies, T., Lege, T., Frechen, M., Franzke, H.J., Brandes, C., 2020. Structural style and neotectonic activity along the Harz Boundary Fault, northern Germany: a multimethod approach integrating geophysics, outcrop data and numerical simulations. International Journal of Earth Sciences, **109**: 1811–1835; https://doi.org/10.1007/s00531-020-01874-0

Muszer, J., Górecka-Nowak, A., Kryza, R., August, C., 2016a. New data on biostratigraphy and chronostratigraphy of the Carboniferous sediments in Sudetes (in Polish). In: XXIII Konferencja Naukowa Sekcji Paleontologicznej Polskiego Towarzystwa Geologicznego (eds. K. Pawłowska and D. Pawłowski): 73–74. Polskie Towarzystwo Geologiczne, Poznań, 21–23.09. 2016.

Muszer, J., Królewiecka, K., Strzoda, A., 2016b. Redeposition of the Upper Visean in the Namurian sediments of Sudetes - examples from Konradów and Jugów (in Polish). In: XXIII Konferencja Naukowa Sekcji Paleontologicznej Polskiego Towarzystwa Geologicznego (eds. K. Pawłowska and D. Pawłowski): 75–76. Polskie Towarzystwo Geologiczne, Poznań, 21–23.09.2016.

Nádaskay, R., Žák, J., Sláma, J., Sidorinová, T., Valečka, J., 2019. Deciphering the Late Paleozoic to Mesozoic tectono sedimentary evolution of the northern Bohemian Massif from detrital zircon geochronology and heavy mineral provenance. International Journal of Earth Sciences, **108**: 2653–2681; https://doi.org/10.1007/s00531-019-01781-z

Nádaskay, R., Valečka, J., Opluštil, S., Mlčoch, B., Skácelová, Z., Horna, F., 2024. Pennsylvanian-Permian deposits in northern Bohemia: a correlation with neighbouring basins and discussion of their formation and demise within the "Elbe Zone System". Geological Quarterly, **68**, 42; https://doi.org/10.7306/gq.1770

Narkiewicz, M., 2007. Development and inversion of Devonian and Carboniferous basins in the eastern part of the Variscan foreland (Poland). Geological Quarterly, **51** (3): 231–256.

Narkiewicz, M., 2020. Variscan foreland in Poland revisited: new data and new concepts. Geological Quarterly, **64** (2): 377–401; http://doi.org/10.7306/gq.1511

Nemec, W., Porębski, S.J., Steel, R.J., 1980. Texture and structure of resedimented conglomerates: examples from Książ Formation (Famennian-Tournaisian), southwestern Poland. Sedimentology, **27**: 519–538; https://doi.org/10.1111/j.1365-3091.1980.tb01645.x

Nemec, W., Porębski, S.J., Teisseyre, A.K., 1982. Explanatory notes to the lithotectonic molasse profile of the Intra-Sudetic Basin, Polish part (Sudety Mts., Carboniferous-Permian). Veröffentlichungen des Zentralinstituts für Physik der Erde, **66**: 267–278.

Novakova, L., 2015. Tectonic phase separation applied to the Sudetic Marginal Fault Zone (NE part of the Czech Republic). Journal of Mountain Science, **12**: 251–267; https://doi.org/10.1007/s11629-014-3297-5

Oberc, J., 1972. Sudety i obszary przyległe (in Polish). In: Budowa Geologiczna Polski. Vol. **4**. Tektonika, Part 2. Wydaw. Geol., Warszawa.

O'Brien, P.J., Kröner, A., Jaeckel, P., Hegner, E., Żelaźniewicz, A., Kryza, R., 1997. Petrological and isotopic studies on Palaeozoic high-pressure granulites, Gory Sowie Mts, Polish Sudetes. Journal of Petrology, **38**: 433–456; https://doi.org/10.1093/petroj/38.4.433

Ostrowski, S., Pacanowski, G., Majer, E., Sokołowska, M., Czarniak, P., Piechota, A., Barański, M., Szabłowska, M., Lasocki, M., Wilkołazki, P., Majer, K., 2023. Badania geologiczno-inżynierskie. Geofizyka Inżynierska (in Polish). Państwowy Instytut Geologiczny – Państwowy Instytut Badawczy, Warszawa.

Pacanowski, G., Maślakowski, M., Lejzerowicz, A., 2021. Practical aspects of field work carried out by Electrical Resistivity Tomography. Archives of Civil Engineering, **68**: 331–346; https://doi.org/10.24425/ace.2022.143041

Pascal, C., 2021. Paleostress Inversion Techniques: Methods and Applications for Tectonics. Elsevier; https://doi.org/10.1016/C2016-0-01840-5

Pešková, I., Hók, J., Štěpančíková, P., Stemberk, J., Vojtko, R., 2010. Results of stress analysis inferred from fault slip data along the Sudetic Marginal Fault (NE part of Bohemian Massif). Acta Geologica Slovaca, **2**: 11–16.

Petit, J.P., 1987. Criteria for the sense of movement on fault surfaces in brittle rocks. Journal of Structural Geology, **9**: 597–608; https://doi.org/10.1016/0191-8141(87)90145-3

Pluta, K., Górecka-Nowak, A., 2018. Miospore evidence for the Carboniferous age of rocks from the Świebodzice Unit (Sudetes, SW Poland). Geological Quarterly, **62** (1): 120–133; https://doi.org/10.7306/gq.1393

Porębski, S.J., 1981. Świebodzice succesion (Upper Devonian-lowest Carboniferous): a prograding, mass flow dominated fan-delta complex (in Polish with English summary). Geologia Sudetica, **21**: 101–192.

Porębski, S.J., 1990. Onset of coarse clastic sedimentation in the Variscan realm of the Sudetes (SW Poland): an example from the upper Devonian-lower Carboniferous Świebodzice succession. Neues Jahrbuch für Geologie und Paläontologie Abhandlungen, **179**: 259–274.

Porras, D., Carrasco, J., Carrasco, P., González, P.J., 2022. Imaging extensional fault systems using deep electrical resistivity tomography: A case study of the Baza fault, Betic Cordillera, Spain. Journal of Applied Geophysics, **202**, 104673; https://doi.org/10.1016/j.jappgeo.2022.104673

Reynolds, J.M., 2011. An Introduction to Applied and Environmental Geophysics. John Wiley & Sons.

Rosenbaum, G., Lister, G.S., Duboz, C., 2002. Relative motions of Africa, Iberia and Europe during Alpine orogeny. Tectonophysics, **359**: 117–129; https://doi.org/10.1016/S0040-1951(02)00442-0

Różycka, M., Jancewicz, K., Migoń, P., Szymanowski, M., 2021. Tectonic versus rock-controlled mountain fronts – geomorphometric and geostatistical approach (Sowie Mts., Central Europe). Geomorphology, **373**, 107485; https://doi.org/10.1016/j.geomorph.2020.107485

Sawicki, L., 1995. Geological Map of Lower Silesia with Adjacent Czech and German Territories (without Quaternary deposits). Państwowy Instytut Geologiczny, Warszawa.

Sheehan, J.R., Doll, W.E., Mandell, W.A., 2005. An evaluation of methods and available software for seismic refraction tomography analysis. Journal of Environmental & Engineering Geophysics, **10**: 21–34.

Sobczyk, A., Szczygieł, J., 2021. Paleostress reconstruction of faults recorded in the Niedźwiedzia Cave (Sudetes): insights into Alpine intraplate tectonic of NE Bohemian Massif. International Journal of Earth Sciences, **110**: 833–847; https://doi.org/10.1007/s00531-021-01994-1

Solecki, A.T., 1994. Tectonics of the North Sudetic Synclinorium. Acta Universitatis Wratislaviensis, **45**: 1–59.

Solecki, A.T., 2011. Structural development of the epi-Variscan cover in the North Sudetic Synclinorium area (in Polish with English summary). In: Mezozoik i kenozoik Dolnego Śląska. LXXXI Zjazdu Polskiego Towarzystwa Geologicznego (eds. A. Żelaźniewicz, J. Wojewoda and W. Cieżkowski): 19–36. WIND.

SPDPSH (System Przetwarzania Danych Państwowej Służby Hydrogeologicznej), 2024. Centralny Bank Danych Hydrogeologicznych (in Polish); https://www.pgi.gov.pl/psh/dane-hydrogeologiczne-psh/947-bazy-danych-hydrogeologiczne/9057-bankhydro.html, accessed: 10-05-2024.

Štěpančíková, P., Dohnal, J., Pánek, T., Łój, M., Smolková, V., Šilhán, K., 2011. The application of electrical resistivity tomography and gravimetric survey as useful tools in an active tectonics study of the Sudetic Marginal Fault (Bohemian Massif, central Europe). Journal of Applied Geophysics, **74**: 69–80; https://doi.org/10.1016/j.jappgeo.2011.03.007

Štěpančíková, P., Hók, J., Nývlt, D., Dohnal, J., Sýkorová, I., Stemberk, J., 2010. Active tectonics research using trenching technique on the south-eastern section of the Sudetic Marginal Fault (NE Bohemian Massif, central Europe). Tectonophysics, **485**: 269–282; https://doi.org/10.1016/j.tecto.2010.01.004

Stephenson, R.A., Narkiewicz, M., Dadlez, R., van Wees, J.-D., Andriessen, P., 2003. Tectonic subsidence modelling of the Polish Basin in the light of new data on crustal structure and magnitude of inversion. Sedimentary Geology, **156**: 59–70; https://doi.org/10.1016/S0037-0738(02)00282-8

Suzuki, K., Toda, S., Kusunoki, K., Fujimitsu, Y., Mogi, T., Jomori, A., 2000. Case studies of electrical and electromagnetic methods applied to mapping active faults beneath the thick quaternary. Engineering Geology, **56**: 29–45; https://doi.org/10.1016/S0013-7952(99)00132-5

Tabaud, A.S., Štípská, P., Mazur, S., Schulmann, K., Míková, J., Wong, J., Sun, M., 2021. Evolution of a Cambro-Ordovician active margin in northern Gondwana: geochemical and zircon geochronological evidence from the Góry Sowie metasedimentary rocks, Poland. Gondwana Research, **90**: 1–26; https://doi.org/10.1016/j.gr.2020.10.011

Teisseyre, A.K., 1975. Sedimentology and palaeogeography of the Kulm alluvial fans in the western Intrasudetic Basin (Central Sudetes, SW Poland) (in Polish with English summary). Geologia Sudetica, **9**: 5–135.

Tomek, F., Vacek, F., Žák, J., Petronis, M.S., Verner, K., Foucher, M.S., 2019. Polykinematic foreland basins initiated during orthogonal convergence and terminated by orogen-oblique strike-slip faulting: An example from the northeastern Variscan belt. Tectonophysics, **766**: 379–397; https://doi.org/10.1016/j.tecto.2019.05.023

Valečka, J., 2019. Jurassic pebbles in the Cretaceous sandstones of the Bohemian Basin as a possible tool for the reconstruction of Late Jurassic and Late Cretaceous paleogeography. Volumina Jurassica, **18**: 17–38; https://doi.org/10.7306/vj.17.2

Van Breemen, O., Bowes, D., Aftalion, M., Żelaźniewicz, A., 1988. Devonian tectonothermal activity in the Sowie Góry gneissic block, Sudetes, southwestern Poland: evidence from Rb-Sr and U-Pb isotopic studies. Annales Societatis Geologorum Poloniae, **58**: 3–19.

Voigt, T., 2009. Die Lausitzer-Riesengebirgs Antiklinalzone als kreidezeitliche inversionsstruktur: geologische Hinweise aus den umgebenden Kreidebecken. Zeitschrift für Geologische Wissenschaften, **37**: 15–39.

Voigt, T., Kley, J., Voigt, S., 2021. Dawn and dusk of Late Cretaceous basin inversion in central Europe. Solid Earth, **12**: 1443–1471; https://doi.org/10.5194/se-12-1443-2021

Wajsprych, B., 1978. Allochthonous Paleozoic rocks in the Visean of the Bardzkie Mts. (Sudetes) (in Polish with English summary). Annales Societatis Geologorum Poloniae, **48**: 99–127.

Ward, S.H., 1987. Electrical Methods in Geophysical Prospecting. In: Geophysics, Methods in Experimental Physics (eds. C.G. Sammis and T.L. Henyey): 265–375. Academic Press; https://doi.org/10.1016/S0076-695X(08)60601-8

Watanabe, T., Matsuoka, T., Ashida, Y., 1999. Seismic traveltime tomography using Fresnel volume approach. SEG Technical Program Expanded Abstracts: 1402–1405. Society of Exploration Geophysicists; https://doi.org/10.1190/1.1820777

Wężyk, P., ed., 2015. Handbook for participants training in the use of LiDAR products (in Polish). Informatyczny System Osłony Kraju przed nadzwyczajnymi zagrożeniami. Główny Urząd Geodezji i Kartografii, Warszawa.

Woźniak, T., Bania, G., 2019. Analysis of the tectonic and sedimentary features of the southern margin of the Krzeszowice Graben in Southern Poland based on an integrated geoelectrical and geological studies. Journal of Applied Geophysics, **165**: 145–151; https://doi.org/10.1016/j.jappgeo.2019.04.010

Zhu, T., Feng, R., Hao, J., Zhou, J., Wang, H., Wang, S., 2009. The Application of Electrical Resistivity Tomography to Detecting a Buried Fault: A Case Study. Journal of Environmental and Engineering Geophysics, **14**: 145–151; https://doi.org/10.2113/JEEG14.3.145

Žák, J., Svojtka, M., Opluštil, S., 2018. Topographic inversion and changes in the sediment routing systems in the Variscan orogenic belt as revealed by detrital zircon and monazite UPb geochronology in post-collisional continental basins. Sedimentary Geology, **377**: 63–81; https://doi.org/10.1016/j.sedgeo.2018.09.008

Żakowa, H., 1960. Horizon Goniatites crenistria from Glinno (Sowie Góry, Sudeten Mts.) (in Polish with English summary). Kwartalnik Geologiczny, **4** (3): 349–366.

Żakowa, H., 1963. Stratigraphy and facial extents of the Lower Carboniferous in the Sudetes (in Polish with English summary). Kwartalnik Geologiczny, **7** (1): 73–94.

Żakowa, H., 1966. Zone Goniatites crenistria Phill. in the vicinity of Sokolec and Jugów, at the foot of the Sowie Mountains (Central Sudetes) (in Polish with English summary). Prace Instytutu Geologicznego, **43**: 1–197.

Żakowa, H., Żak, C., 1962. Lower Carboniferous at Kamionki (Sowie Mts. - Lower Silesia) (in Polish with English summary). Biuletyn Instytutu Geologicznego, **173**: 169–277.

Żelaźniewicz, A., 1987. Tectonic and metamorphic evolution of the Sowie Góry, Sudetes Mts., SW Poland (in Polish with English summary). Annales Societatis Geologorum Poloniae, **57**: 203–348.

Żelaźniewicz, A., 1990. Deformation and metamorphism in the Góry Sowie gneiss complex, Sudetes, SW Poland. Neues Jahrbuch für Geologie und Paläontologie Abhandlungen, **179**: 129–157.